Journal of Medicinal Chemistry



Article

# Development of 2-(2-(3-(4-([18F]Fluoromethoxy-d2)phenyl)-7-methyl- 4-oxo-3,4-dihydroquinazolin-2-yl)ethyl)-4-isopropoxyisoindoline-1,3-dione for Positron Emission Tomography Imaging of Phosphodiesterase 10A (PDE10A) in Brain

Wakana Mori, Tomoteru Yamasaki, Masayuki Fujinaga, Masanao Ogawa, Yiding Zhang, Akiko Hatori, Lin Xie, Katsushi Kumata, Hidekatsu Wakizaka, Yusuke Kurihara, Takayuki Ohkubo, Nobuki Nengaki, and Ming-Rong Zhang

*J. Med. Chem.*, **Just Accepted Manuscript** • DOI: 10.1021/acs.jmedchem.8b01366 • Publication Date (Web): 05 Dec 2018



ACS Publications

is published by the American Chemical Society. 1155 Sixteenth Street N.W., Washington, DC 20036

# Development of 2-(2-(3-(4-([$^{18}$F]Fluoromethoxy-$d_2$)phenyl)-7-methyl-4-oxo-3,4-dihydroquinazolin-2-yl)ethyl)-4-isopropoxyisoindoline-1,3-dione for Positron Emission Tomography Imaging of Phosphodiesterase 10A (PDE10A) in Brain

Wakana Mori,[†,∥] Tomoteru Yamasaki,[†,∥] Masayuki Fujinaga,[†] Masanao Ogawa,[†,‡] Yiding Zhang,[†] Akiko Hatori,[†] Lin Xie,[†] Katsushi Kumata,[†] Hidekatsu Wakizaka,[§] Yusuke Kurihara,[†,‡] Takayuki Ohkubo,[†,‡] Nobuki Nengaki,[†,‡] and Ming-Rong Zhang[†,*]

[†]Department of Radiopharmaceuticals Development, National Institute of Radiological Sciences, National Institutes for Quantum and Radiological Science and Technology, 4-9-1 Anagawa, Inage-ku, Chiba, 263-8555, Japan

[‡]SHI Accelerator Service, Ltd, 1-17-6 Osaki, Shinagawa-ku, Tokyo, 141-0032, Japan

[§]Department of Radiation Measurement and Dose Assessment, National Institute of Radiological Sciences, National Institutes for Quantum and Radiological Science and Technology, 4-9-1 Anagawa, Inage-ku, Chiba, 263-8555, Japan

***Corresponding author:**

Ming-Rong Zhang, PhD

Department of Radiopharmaceuticals Development, National Institute of Radiological Sciences, National Institutes for Quantum and Radiological Science and Technology, 4-9-1 Anagawa, Inage-ku, Chiba 263-8555, Japan

Tel: +81 43 382 3709; Fax: +81 43 206 3261

E-mail: zhang.ming-rong@qst.go.jp

## ABSTRACT

Phosphodiesterase 10A (PDE10A) is a newly identified therapeutic target for central nervous system disorders. 2-(2-(3-(4-([$^{18}$F]Fluoroethoxy)phenyl)-4-oxo-3,4-dihydroquinazolin-2-yl)ethyl)-4-isopropoxyisoindoline-1,3-dione ([$^{18}$F]MNI-659, [$^{18}$F]**5**) is a useful positron emission tomography (PET) ligand for imaging of PDE10A in the human brain. However, the radiolabeled metabolite of [$^{18}$F]**5** can accumulate in the brain. In this study, using [$^{18}$F]**5** as a lead compound, we designed four new $^{18}$F-labeled ligands ([$^{18}$F]**6**–**9**) to find one more suitable than [$^{18}$F]**5**. Of these, 2-(2-(3-(4-([$^{18}$F]fluoromethoxy-$d_2$)phenyl)-4-oxo-3,4-dihydroquinazolin-2-yl)ethyl)-4-isopropoxyisoindoline-1,3-dione ([$^{18}$F]**9**) exhibited high in vitro binding affinity ($K_i$ = 2.9 nM) to PDE10A and suitable lipophilicity (LogD = 2.2). In PET studies, the binding potential ($BP_{ND}$) of [$^{18}$F]**9** (5.8) to PDE10A in rat brains was significantly higher than that of [$^{18}$F]**5** (4.6). Furthermore, metabolite analysis showed much lower levels of contamination with radiolabeled metabolites of [$^{18}$F]**9** in the brain than those of [$^{18}$F]**5**. In conclusion, [$^{18}$F]**9** is a useful PET ligand for PDE10A imaging in brain.

## INTRODUCTION

Cyclic nucleotide signaling regulates a wide variety of cellular functions. Phosphodiesterases (PDEs) act in every known neuronal population by catalyzing the breakdown of 3',5'-cyclic adenosine monophosphate or 3',5'-cyclic guanosine monophosphate (cGMP) and are characterized into 12 superfamilies according to enzymatic characteristics, distribution, and pharmacological profile.[1–4] Among these, PDE10A is newly identified and contains two amino-terminal domains that are similar to the cGMP-binding domains of PDE2, PDE5, and PDE6 and that are highly expressed in medium spiny neurons in the striatum.[1,5,6] Because of the localization and regulatory functions of PDE10A, therapeutic studies have been conducted to investigate the effects of PDE10A inhibitors on multiple central nervous system disorders, such as schizophrenia, Huntington's disease, and Parkinson's disease (PD).[7–11] Moreover, the biological importance of PDE10A expression in PD progression and severity has been reported.[12] Despite the behavioral and biological studies that have been conducted, direct evidence on the interaction between PDE10A functions and multiple neurodegenerative and neuropsychiatric diseases is scarce.

Positron emission tomography (PET) imaging with radioligands specific to targeted molecules is frequently used to visualize in vivo brain activity related to the

targeted molecules and provide detailed in vivo information about their relationship with brain functions and diseases. Since 2010, some research groups have developed carbon-11 ($^{11}$C)- or fluorine-18 ($^{18}$F)-labeled radioligands for PDE10A in the brain, some of which have shown some promising results in preclinical PET imaging studies.[13–29] To the best of our knowledge, the following five PET ligands have been used for visualization of PDE10A in the human brain to date: 1-[2-fluoro-4-(tetrahydro-2*H*-pyran-4-yl)phenyl]-5-[$^{11}$C]methoxy-3-(1-phenyl-1*H*-pyrazol-5-yl)pyridazin-4(1*H*)-one ([$^{11}$C]T-773, [$^{11}$C]**1**),[30] 5,8-dimethyl-2-[2-((1-[$^{11}$C]methyl)-4-phenyl-1*H*-imidazol-2-yl)-ethyl]-[1,2,4]triazolo[1,5-*a*]pyridine ([$^{11}$C]Lu-AE92686, [$^{11}$C]**2**),[31] ((*R*)-5-(3-fluoropyrrolidin-1-yl)-2-(3-methylquinoxalin-2-yl)-*N*-[$^{11}$C]methyl-*N*-(tetrahydro-2*H*-pyran-4-yl)pyrazolo[1,5-*a*]pyrimidin-7-amine) ([$^{11}$C]IMA107, [$^{11}$C]**3**),[12,32–35] 2-[[4-[1-(2-$^{18}$F-fluoroethyl)-4-(4-pyridinyl)-1*H*-pyrazol-3-yl]phenoxy]methyl]-3,5-dimethylpyridine ([$^{18}$F]JNJ42259152, [$^{18}$F]**4**),[36,37] and 2-(2-(3-(4-([$^{18}$F]fluoroethoxy)phenyl)-4-oxo-3,4-dihydroquinazolin-2-yl)ethyl)-4-isopropoxyisoindoline-1,3-dione ([$^{18}$F]MNI-659, [$^{18}$F]**5**) (Figure 1).[19,38–41]

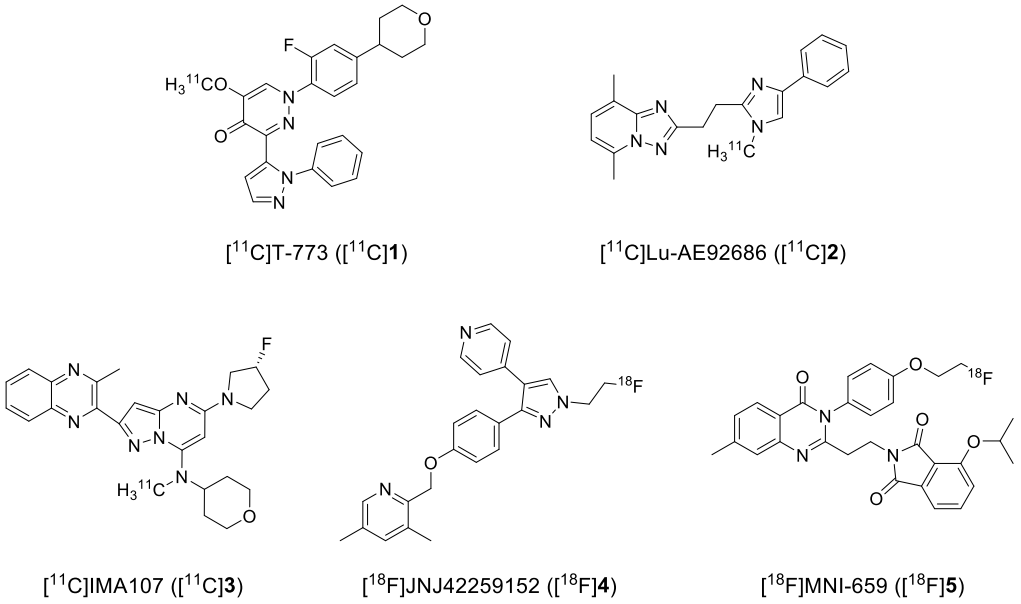


**Figure 1.** PET radioligands for clinical PDE10A imaging.

In general, $^{18}$F-labeled ligands give higher quality PET images with higher spatial resolution than $^{11}$C-ligands. Moreover, $^{18}$F is convenient for multi-scans, storage and transportation to other facilities. Among the PDE10A radioligands, [$^{18}$F]**4** and [$^{18}$F]**5** are more convenient for PET measurement than [$^{11}$C]**1**–**3**. Compared to [$^{18}$F]**4**, [$^{18}$F]**5** is frequently used for PDE10A imaging in human studies because of its promising results of first-in-human study.[19] PET with [$^{18}$F]**5** showed high in vivo availability ($BP_{ND}$) in the human brain.[38] However, PET quantitative assessments with [$^{18}$F]**5** have shown varying results. For example, the coefficient of variation (CV) in measurements of the binding potential ($BP_{ND}$) of [$^{18}$F]**5** with the Logan graphical method was higher than 30% in non-human primate brains.[42] Further, it was reported that some PET ligands containing a 2-

[$^{18}$F]fluoroethoxy group are easily metabolized via the Cytochrome P450 monooxygenase system in the liver, resulting in [$^{18}$F]fluoroacetaldehyde.[43,44] Subsequently, [$^{18}$F]fluoroacetaldehyde is rapidly oxidized to [$^{18}$F]fluoroacetate, which is easily accumulated in brain and has even been used as an imaging tool for detection of cerebral ischemia.[45,46] Thus, high variation in quantitative PET measurements of [$^{18}$F]**5** may be caused by contamination with [$^{18}$F]fluoroacetate in the brain.

In this study, we aimed to develop a more suitable PET ligand for quantification of PDE10A concentrations than [$^{18}$F]**5**. Using **5** as a lead compound, we designed four new fluoroalkyloxy candidates, **6**–**9**, and subsequently radiolabeled them with $^{18}$F (Figure 2). In place of the fluoroethoxy group in [$^{18}$F]**5**, a 3-fluoropropoxy, (3-fluoro-2-hydroxy)propoxy, fluoromethoxy, or fluoromethoxy-$d_2$ group was introduced to generate the new radioligands [$^{18}$F]**6**–**9**. Introduction of [$^{18}$F]fluoroalkyloxy groups may reduce contamination of the brain with radiolabeled metabolites by avoiding the production of [$^{18}$F]fluoroacetate.

Herein, we perform the chemical syntheses of **6**–**9**, radiosyntheses of [$^{18}$F]**6**–**9**, in vitro binding assays with PDE10A, and in vivo PET imaging studies of the four radioligands. To validate their usefulness, we further conducted biodistribution studies and metabolite analyses of [$^{18}$F]**8** and [$^{18}$F]**9**. Although [$^{18}$F]**5** has been used in clinical

studies, detailed preclinical data including in vivo metabolite analysis in brain have not been reported. We report the results of a preclinical evaluation of [$^{18}$F]**5** in rodents for the first time and compare the results with those of [$^{18}$F]**6**–**9**.

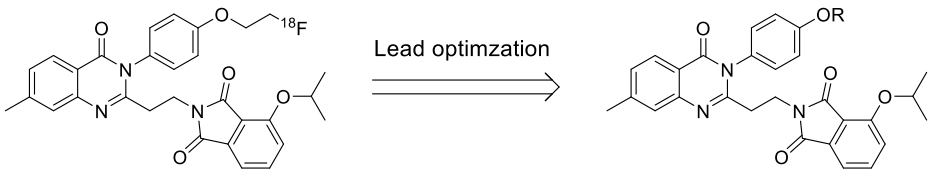


**[$^{18}$F]5**

**6**: R = $CH_2CH_2CH_2F$
**[$^{18}$F]6**: R = $CH_2CH_2CH_2{}^{18}F$
**7**: R = $CH_2CH(OH)CH_2F$
**[$^{18}$F]7**: R = $CH_2CH(OH)CH_2{}^{18}F$
**8**: R = $CH_2F$
**[$^{18}$F]8**: R = $CH_2{}^{18}F$
**9**: R = $CD_2F$
**[$^{18}$F]9**: R = $CD_2{}^{18}F$

**Figure 2.** Chemical structures of compounds **6**–**9** and PET ligands [$^{18}$F]**6**–**9** in this study.

## RESULTS AND DISCUSSION

### Chemistry

The novel fluoroalkyloxy analogs **6**–**9** were synthesized using the same desmethyl phenol precursor: 2-(2-(3-(4-hydroxyphenyl)-4-oxo-3,4-dihydroquinazolin-2-yl)ethyl)-4-isopropoxyisoindoline-1,3-dione (**10**)[47] (Scheme 1, Supplemental Information Table S1 and Figure S1). The reactions of **10** with fluoropropyl tosylate (**11**) and fluoromethyl tosylate (**13**) in the presence of $K_2CO_3$ at 70° C produced **6** and **8** with 52% and 60%

yields, respectively. The cycle-opening reaction of epifluorohydrin **12** with **10** and $K_2CO_3$

**Scheme 1.** Chemical synthesis of compounds **6–9**[a]

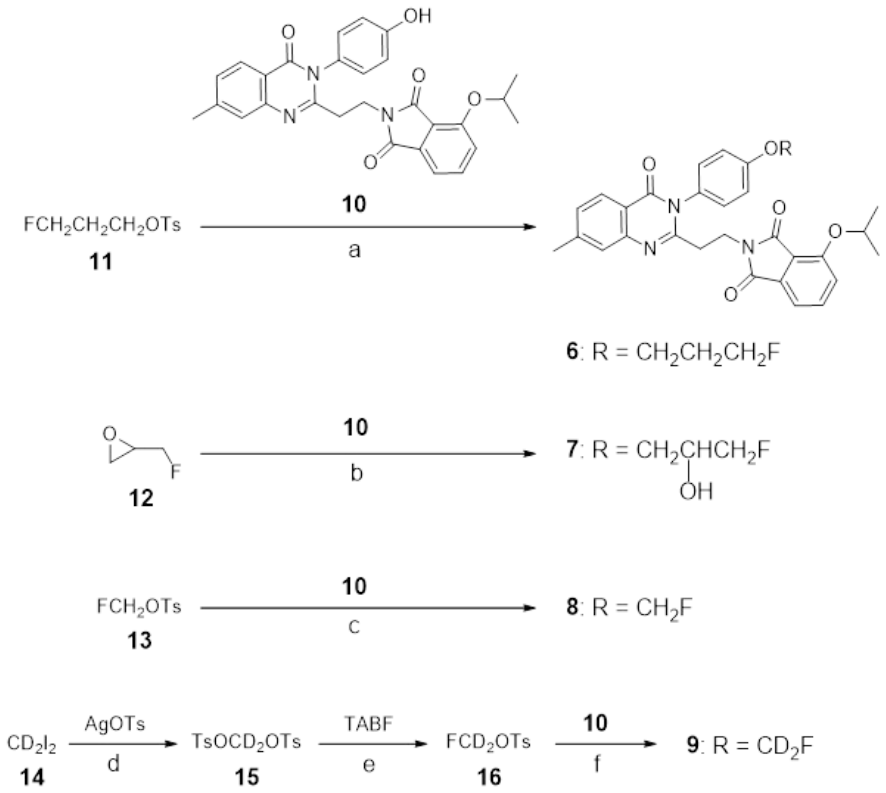


[a]Reagents and conditions: (a) $K_2CO_3$, DMF, 70° C, 11 h; (b) $K_2CO_3$, DMF, 80° C, 18 h; (c) $K_2CO_3$, DMF, 70° C, 18 h; (d) silver *p*-toluenesulfonate, $CH_3CN$, reflux, 18 h; (e) TBAF, $CH_3CN$, reflux, 12 h; (f) $K_2CO_3$, DMF, 70° C, 13 h.

at 80° C for 18 h produced **7**, which contains the (3-fluoro-2-hydroxy)propoxy group. To prepare the fluoromethoxy-$d_2$ analog **9**, fluoromethyl-$d_2$ tosylate (**16**) was synthesized by a unique route[48]. Diiodomethane-$d_2$ (**14**) was heated with silver tosylate in acetonitrile ($CH_3CN$) to generate bis(tosyloxy)methane-$d_2$ (**15**), followed by treatment with tetrabutylammonium fluoride (TBAF) to yield **16**. Similarly to **8**, compound **9** was synthesized by fluoromethylation of **10** with **16** and $K_2CO_3$; this process had 24% yield.

**In vitro Profiles of PET Ligand Candidates for PDE10A**

The in vitro binding affinities of PET ligand candidates for PDE10A **6–9** were measured using a binding assay with [$^{18}$F]**5** in rat brain homogenates. These compounds exhibited binding affinities ($K_i$) for PDE10A on the single-digit nM order, with a range of 2.6–8.1 nM (Table 1). Changing the fluoroethoxy group to the relatively large fluoropropoxy group in **6** or 3-fluoro-2-hydroxypropoxy group in **7** slightly weakened affinities for PDE10A. The $K_i$ values of **8** and **9** with fluoromethoxy and fluoromethoxy-$d_2$ groups remained 2.6 and 2.9 nM, respectively, which were slightly stronger than that of **5** (MNI-659: 3.0 nM). These results suggest that only relatively small moieties substituted at the 4-position of the benzene ring in these analogs can fit into the PDE10A domain's binding site.

The values of lipophilicity (LogD) were measured by the shake flask method,[49] as shown in Table 1. The LogD values of [$^{18}$F]**5–9** following radiolabeling with $^{18}$F were 2.2–2.9. These values are in the range normally considered as suitable for PET ligands in brain imaging.[50] When the size of the fluoroalkyl group shrank, lipophilicity was also reduced in this series of compounds.

**Table1.** In vitro binding affinity and lipophilicity of compounds **6–9**.

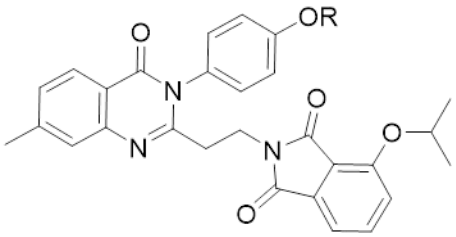


| Compounds | R | Ki (nM)[a] | Lipophilicity (LogD)[a] |
|---|---|---|---|
| **6** | $CH_2CH_2CH_2F$ | 4.2 (2.3–7.4) | 2.90 (2.85–2.94) |
| **7** | $CH_2CH(OH)CH_2F$ | 8.1 (3.3–15.3) | 2.83 (2.81–2.85) |
| **8** | $CH_2F$ | 2.6 (1.5–4.6) | 2.29 (2.28–2.30) |
| **9** | $CD_2F$ | 2.9 (1.5–5.3) | 2.15 (2.14–2.16) |
| **5** (MNI-659) | $CH_2CH_2F$ | 3.0 (1.9–5.0) | 2.48 (2.43–2.52) |

[a]Assays were duplicated.

Because of these compounds' promising in vitro profiles, we radiolabeled **6–9** with $^{18}F$ and performed in vivo evaluation of PET imaging of PDE10A in rat brain.

## Radiochemistry

Radiosyntheses of [$^{18}F$]**6–9** were performed using a homemade automated synthesis system[51] (Scheme 2). Our automated system included two steps: 1) preparation

of [$^{18}$F]fluoroalkylating agents[52]: [$^{18}$F]fluoropropyl bromide ([$^{18}$F]**17**),[53] [$^{18}$F]epifluorohydrin ([$^{18}$F]**12**),[54] [$^{18}$F]fluoromethyl bromide ([$^{18}$F]**18**),[48] and [$^{18}$F]fluoromethyl bromide-$d_2$ ([$^{18}$F]**19**)[55]; 2) reaction of phenol precursor **10** with the [$^{18}$F]fluoroalkylating agents. As the first step, the [$^{18}$F]fluoroalkylating agents were produced by [$^{18}$F]fluorination of triflate **20**, tosylate **21**, or bromides **22** or **23** with [$^{18}$F]$F^-$. After the [$^{18}$F]fluorination, [$^{18}$F]**17** (boiling point [bp]: 61° C) or [$^{18}$F]**12** (bp: 84° C) was distilled from the reaction mixture and directly trapped into another reaction vessel for the following [$^{18}$F]fluoroalkylation. As for [$^{18}$F]**18** (bp: 15° C) or [$^{18}$F]**19** (bp: 15° C), the crude [$^{18}$F]fluorinating products were distilled from the reaction mixture, immediately passed through three short silica Sep-Pak columns to delete volatile unreacted **22** or **23**, and trapped in another vessel for [$^{18}$F]fluoroalkylation.

The reactions of **10** with [$^{18}$F]**17**, [$^{18}$F]**12**, [$^{18}$F]**18**, or [$^{18}$F]**19** were heated at 90–130° C for 5–20 min. Utilization of these distilled [$^{18}$F]fluoroalkylating agents resulted in clear reaction mixtures. Moreover, as compared with the conventional tosylate precursor used for direct [$^{18}$F]fluorination, only 1–2 mg of phenol **10** was sufficient for efficient [$^{18}$F]fluoroalkylation. Under the automated synthesis system, [$^{18}$F]**6–9** were easily separated from the reaction mixtures using semi-preparative reversed phase HPLC (Supplemental Information Figure S2). After HPLC separation and formulation, [$^{18}$F]**6**

(0.24–0.35 GBq) or [$^{18}$F]**7** (0.10–0.13 GBq) was produced as an injectable solution with 4% ± 1% (n = 3) and 2% (average, n = 2) radiochemical yields at the end of synthesis (EOS), starting from the cyclotron-produced [$^{18}$F]$F^-$ radioactivity of 7.4 GBq. In addition, [$^{18}$F]**8** (0.59–0.88 GBq) and [$^{18}$F]**9** (0.66–0.94 GBq) were produced with 7% ± 2% (n = 7) and 7% ± 3% (n = 9) radiochemical yields at EOS, respectively, starting from [$^{18}$F]$F^-$ radioactivity of 12.3–15.6 GBq. Because of the difference in electrophilicity between the [$^{18}$F]fluoromethyl and [$^{18}$F]fluoropropyl groups, [$^{18}$F]**18** and [$^{18}$F]**19** showed higher reactivity with phenol **10** than [$^{18}$F]**17** and [$^{18}$F]**12** did. In the finally formulated product solutions, the molar activities and radiochemical purities of [$^{18}$F]**6**–**9** were 200–400 GBq/μmol and greater than 99% at EOS (Supplemental Information Figure S3). Moreover, these products did not show radiolysis at room temperature for 120 min after formulation, indicating their radiochemical stability within the duration of at least one PET scan. All of the analytical results of [$^{18}$F]**6**–**9** were in compliance with our in-house quality control/assurance specifications for radiopharmaceuticals produced in our facility for preclinical and clinical uses.

**Scheme 2.** Radiosynthesis of [$^{18}$F]**6–9**[a]

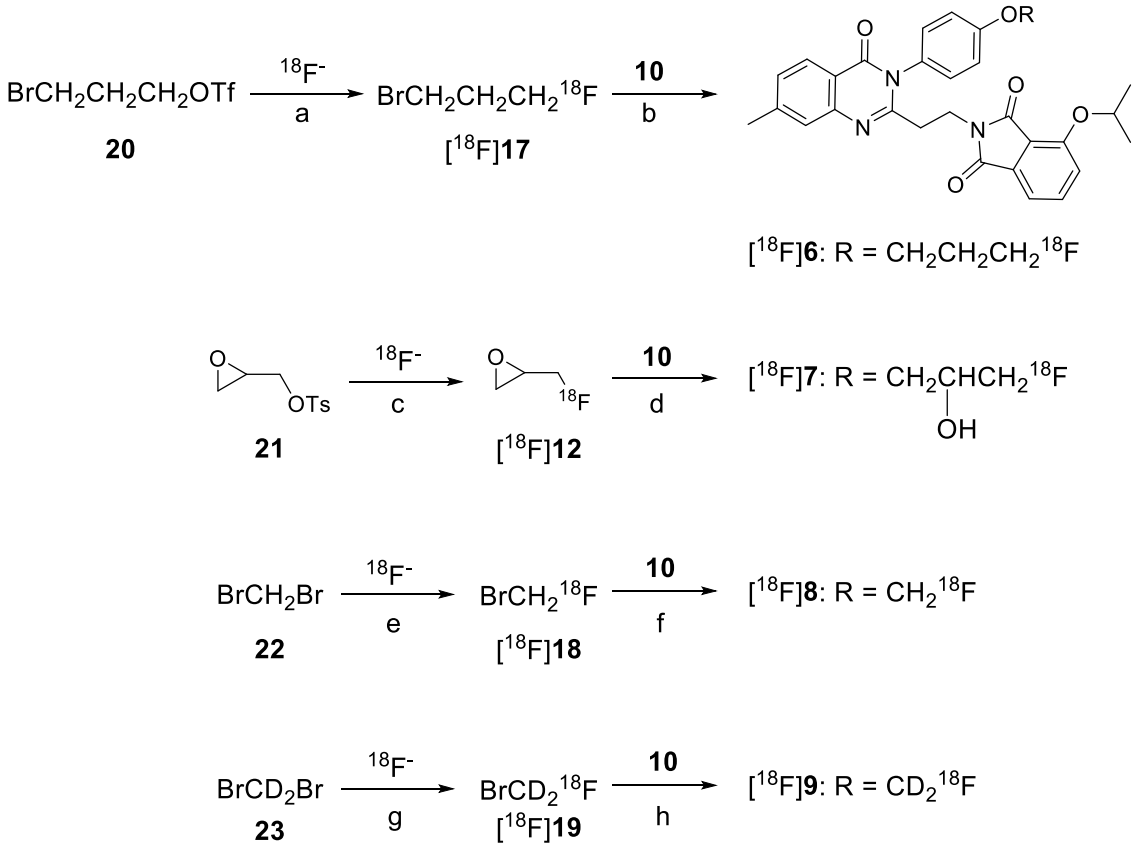


[a]Reagents and conditions: (a) *o*-dichlorobenzene, 130° C, 2 min; (b) NaOH, DMF, 120° C, 10 min; (c) *o*-dichlorobenzene, 130° C, 2 min; (d) NaOH, DMF, 130° C, 20 min; (e) $CH_3CN$, 100° C, 5 min; (f) NaOH, DMF, 90° C, 5 min; (g) $CH_3CN$, 100° C, 5 min; (h) NaOH, DMF, 90° C, 5 min.

## Small-Animal PET Assessments

Figure 3 shows averaged PET/MRI images (A) and tissue time–activity curves (tTACs) (B) of [$^{18}$F]**5–9** in rat brains. It has been reported that PDE10A mRNA can be heterogeneously detected in the brain.[56,57] The highest expression of PDE10A has been shown in the striatum. On the other hand, negligible PDE10A levels have been found in

the mid-brain and pons.[57]

As shown in the PET images, [$^{18}$F]**6**, [$^{18}$F]**8**, and [$^{18}$F]**9** showed a similar distribution of radioactivity to the PDE10A-specific [$^{18}$F]**5**. Significant radioactivity was observed in the striatum. No uptake was observed in other brain regions. The images reflecting significant striatal uptake were similar to the PET rat brain image using [$^{11}$C]**1** (Figure 1), a PDE10A-specific radioligand, as reported previously.[58] These results suggested that current PET ligands may have specific binding for striatal PDE10A but not for other brain region's PDE10A at low density.

Radioactive uptake in the striatum had the following rank order: [$^{18}$F]**8** ≈ [$^{18}$F]**9** > [$^{18}$F]**5** > [$^{18}$F]**6** > [$^{18}$F]**7** (Figure 3A). The sequence of these radiologands' striatal uptake was constituent with that of their in vitro binding affinities to PDE10A. To our surprise, the striatal uptake of [$^{18}$F]**7** was negligible (< 0.3 SUV). Although the in vitro binding affinity of **7** with PDE10A was the weakest among the present radioligands, its affinity ($K_i$ = 8.1 nM) is still considered relatively strong. These results suggest that brain uptake of [$^{18}$F]**7** may be limited by blood-brain barrier, resulting in a very low initial uptake of radioactivity.

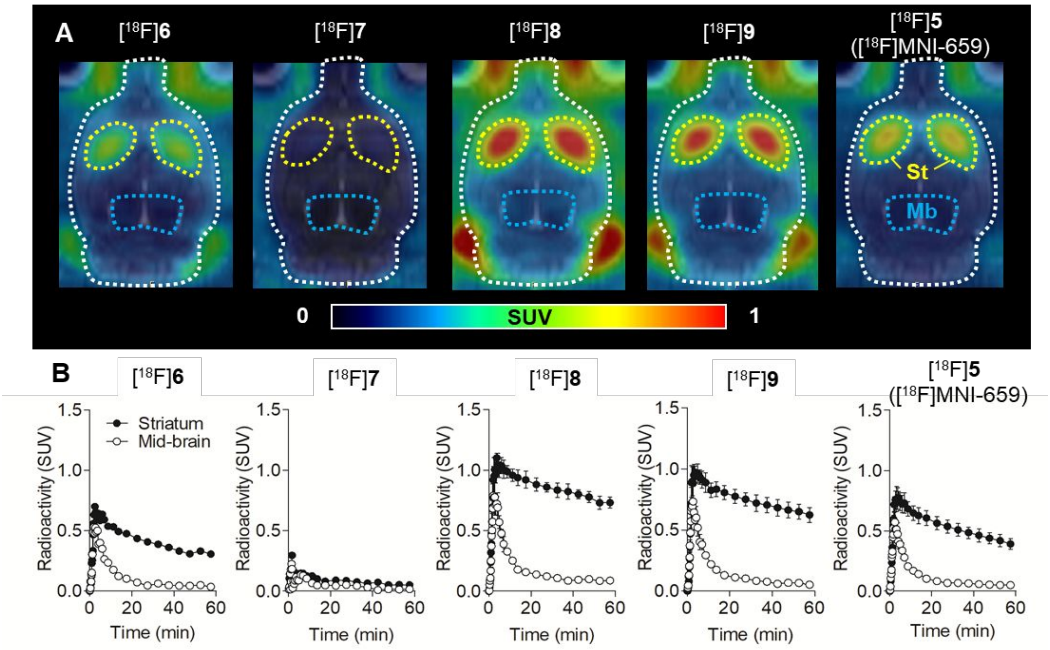


**Figure 3.** Averaged PET/MRI images (A) and tTACs (B) of [$^{18}$F]**5**–**9**. Horizontal PET images were reconstructed by summation between 0 and 60 min. The tTACs were obtained from ROIs located on the striatum (filled circles) and midbrain (open circles). Radioactivity is expressed as standardized uptake value (SUV). St, striatum; Mb, mid-brain.

In contrast, there were very low levels of radioactivity in the mid-brain during the PET scans for each radioligand. Thus, noninvasive PET kinetic analyses for estimation of ligand availability to PDE10A, represented as $BP_{ND}$ in the current PET studies, were performed using the tTAC of the midbrain as a reference region.

Table 2 shows the striatal kinetic parameters (R1 and $BP_{ND}$) based on the simplified reference tissue model (SRTM)[59] using the tTAC of the mid-brain as a reference region. Parameter R1 (= $K_1/K_1$', the ratio of tracer delivery) was 1.0 for all

radioligands except [$^{18}$F]**7**, which indicated equal input functions ($K_1$) in both the interest (striatum) and reference (midbrain) regions. The $BP_{ND}$ values of the two [$^{18}$F]fluoromethoxy radioligands were 5.6 for [$^{18}$F]**8** and 5.8 for [$^{18}$F]**9**. The values were significantly higher ($P < 0.01$ for [$^{18}$F]**8** and [$^{18}$F]**9**) than that of the lead compound [$^{18}$F]**5** (4.6), although the difference between the three compounds' in vitro affinities was small.

Because of the very low $BP_{ND}$ values of [$^{18}$F]**6** and [$^{18}$F]**7** for visualizing PDE10A, we ceased evaluation of those two radioligands in the following studies.

**Table 2.** In vivo availability ($BP_{ND}$) of [$^{18}$F]**5**–**9** to PDE10A (Mean ± s.d.)

| Parameters | [$^{18}$F]**6** (n = 1) | [$^{18}$F]**7** (n = 1) | [$^{18}$F]**8** (n = 3) | [$^{18}$F]**9** (n = 5) | [$^{18}$F]**5** (n = 4) |
|---|---|---|---|---|---|
| R1 | 1.0 | 0.3 | 1.0 ± 0.2 | 1.0 ± 0.1 | 1.0 ± 0.1 |
| $BP_{ND}$ | 3.8 | 0.6 | 5.6 ± 0.5** | 5.8 ± 0.2*** | 4.6 ± 0.6 |

**P < 0.01, ***P < 0.001 (vs [$^{18}$F]**5**)

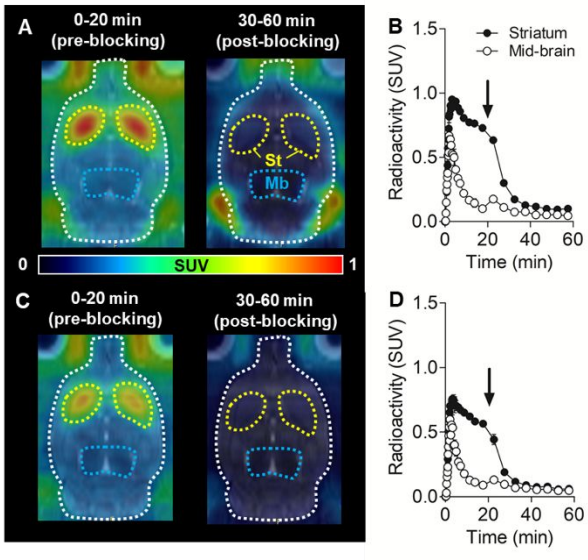

**Figure 4.** Averaged PET/MRI images and tTACs in chase-blocking study for [$^{18}$F]**9** (A and B) and [$^{18}$F]**5** (C and D). Blocking agent (MNI-659 of 5 mg/kg) was administrated 20 min after the injection of the radioligand (black arrows). Horizontal PET images were reconstructed in summation of pre-administration (0-20 min) and post-administration (30–60 min), respectively. The tTACs were obtained from ROIs located on the striatum (filled circles) and mid-brain (open circles). Radioactivity is expressed as SUV. St, striatum; Mb, mid-brain.

To confirm specific binding to PDE10A, chase-blocking PET studies for [$^{18}$F]**9** and [$^{18}$F]**5** were performed. Figure 4 shows PET images and tTACs in the brains of rats administrated with unlabeled **5** (MNI-659, 5 mg/kg) 20 min after the injection of [$^{18}$F]**9** (A and B) and [$^{18}$F]**5** (C and B). In both PET images of the post-blocking, high radioactive signals in the striatum were significantly washed out compared to the pre-blocking (Figs. 4A and C). Radioactivity in the striatum was decreased to 0.1 SUV in both radioligands by administration with the blocking agent. These results suggest that radioactive accumulation in the striatum indicated specific binding of radioligand for PDE10A.

**Biodistribution and Dosimetric Studies**

To evaluate the potent availability of [$^{18}$F]**8** and [$^{18}$F]**9** to PDE10A, their biodistribution throughout the whole body of mice and effective doses of radioactivity were compared with those of [$^{18}$F]**5**. Tables 3–5 show the radioactive concentrations

(%ID/g) of [$^{18}$F]**8**, [$^{18}$F]**9**, and [$^{18}$F]**5** at various time points (5, 15, 30, 60, and 120 min) in each tissue. These radioligands showed similar distribution patterns of radioactivity throughout the whole body of mice. At 5 min after radioligand injection, radioactive uptake was mainly distributed in the small intestine and liver, which reached roughly 60%ID/g. Subsequently, these organs' radioactivities decreased with time after the initial accumulation. Their relatively low renal uptake suggests that these radioligands are eliminated by enterohepatic circulation. At 60 min, the radioactivity levels in all tissues except the small intestine and stomach had decreased to <1%ID/g.

In general, low bone uptake is a requirement for useful $^{18}$F-labelled ligands.[60] Low uptake values (0.58–0.77%ID/g) in bone were determined at 5 min after radioligand injection. The radioactive bone accumulation of [$^{18}$F]**5** decreased to a very low value (0.1%ID/g) until 120 min. Although the radioactive accumulations of [$^{18}$F]**8** and [$^{18}$F]**9** in bone gradually increased with time, their bone uptakes maintained a low level of 1%ID/g at 120 min. These results suggest that in vivo defluorination of the two fluoromethoxy ligands was not significant.

**Table 3.** Biodistribution (%ID/g tissue) of [$^{18}$F]**8** in mice (Mean ± s.d., n = 3).

| Tissue | Time after injection | | | | |
|---|---|---|---|---|---|
| | 5 min | 15 min | 30 min | 60 min | 120 min |
| Blood | 0.88 ± 0.32 | 0.36 ± 0.04 | 0.19 ± 0.03 | 0.06 ± 0.01 | 0.03 ± 0.01 |
| Heart | 1.01 ± 0.35 | 0.37 ± 0.02 | 0.20 ± 0.03 | 0.07 ± 0.02 | 0.03 ± 0.00 |
| Lung | 1.24 ± 0.43 | 0.44 ± 0.04 | 0.22 ± 0.04 | 0.08 ± 0.02 | 0.05 ± 0.02 |
| Liver | 11.01 ± 1.01 | 4.83 ± 0.28 | 1.45 ± 0.27 | 0.70 ± 0.04 | 0.54 ± 0.36 |
| Pancreas | 1.12 ± 0.31 | 0.42 ± 0.03 | 0.18 ± 0.01 | 0.08 ± 0.02 | 0.03 ± 0.00 |
| Spleen | 0.77 ± 0.14 | 0.28 ± 0.04 | 0.17 ± 0.05 | 0.05 ± 0.01 | 0.02 ± 0.00 |
| Kidney | 2.19 ± 0.47 | 0.87 ± 0.17 | 0.48 ± 0.10 | 0.16 ± 0.02 | 0.08 ± 0.01 |
| Stomach | 0.71 ± 0.38 | 5.45 ± 5.85 | 4.09 ± 2.11 | 8.53 ± 6.16 | 2.08 ± 0.45 |
| S. Intestine | 49.50 ± 11.14 | 38.25 ± 9.87 | 16.71 ± 5.48 | 21.21 ± 4.13 | 7.47 ± 3.12 |
| L. Intestine | 1.03 ± 0.28 | 0.60 ± 0.07 | 0.29 ± 0.04 | 0.37 ± 0.29 | 0.05 ± 0.02 |
| Testis | 0.40 ± 0.10 | 0.24 ± 0.01 | 0.15 ± 0.04 | 0.14 ± 0.11 | 0.04 ± 0.01 |
| Muscle | 0.59 ± 0.27 | 0.37 ± 0.22 | 0.21 ± 0.01 | 0.10 ± 0.07 | 0.04 ± 0.01 |
| Brain | 0.56 ± 0.06 | 0.32 ± 0.04 | 0.21 ± 0.05 | 0.15 ± 0.03 | 0.09 ± 0.01 |
| Bone | 0.62 ± 0.12 | 0.58 ± 0.01 | 0.91 ± 0.25 | 0.87 ± 0.21 | 1.06 ± 0.13 |

**Table 4.** Biodistribution (%ID/g tissue) of [$^{18}$F]**9** in mice (Mean ± s.d., n = 3).

| Tissue | Time after injection | | | | |
|---|---|---|---|---|---|
| | 5 min | 15 min | 30 min | 60 min | 120 min |
| Blood | 1.12 ± 0.14 | 0.38 ± 0.05 | 0.24 ± 0.07 | 0.11 ± 0.01 | 0.04 ± 0.01 |
| Heart | 1.24 ± 0.17 | 0.52 ± 0.12 | 0.28 ± 0.07 | 0.12 ± 0.02 | 0.04 ± 0.00 |
| Lung | 1.60 ± 0.31 | 0.60 ± 0.09 | 0.33 ± 0.09 | 0.13 ± 0.02 | 0.05 ± 0.01 |
| Liver | 13.02 ± 1.75 | 4.53 ± 0.90 | 1.92 ± 0.22 | 1.03 ± 0.16 | 0.89 ± 0.29 |
| Pancreas | 1.50 ± 0.28 | 0.49 ± 0.08 | 0.28 ± 0.06 | 0.14 ± 0.00 | 0.06 ± 0.03 |
| Spleen | 1.00 ± 0.19 | 0.35 ± 0.09 | 0.20 ± 0.02 | 0.09 ± 0.01 | 0.03 ± 0.01 |
| Kidney | 3.03 ± 0.82 | 1.23 ± 0.25 | 0.78 ± 0.22 | 0.31 ± 0.04 | 0.10 ± 0.01 |
| Stomach | 2.06 ± 2.00 | 3.08 ± 3.60 | 1.16 ± 0.71 | 2.37 ± 1.38 | 1.98 ± 1.52 |
| S. Intestine | 46.20 ± 9.69 | 37.00 ± 6.83 | 19.63 ± 1.36 | 9.21 ± 0.28 | 10.18 ± 4.63 |
| L. Intestine | 1.46 ± 0.54 | 0.46 ± 0.08 | 0.22 ± 0.02 | 0.31 ± 0.14 | 0.99 ± 1.07 |
| Testis | 0.60 ± 0.15 | 0.31 ± 0.05 | 0.20 ± 0.01 | 0.10 ± 0.03 | 0.04 ± 0.02 |
| Muscle | 1.01 ± 0.15 | 0.30 ± 0.04 | 0.31 ± 0.07 | 0.10 ± 0.02 | 0.05 ± 0.01 |
| Brain | 0.73 ± 0.15 | 0.37 ± 0.06 | 0.27 ± 0.02 | 0.18 ± 0.01 | 0.11 ± 0.01 |
| Bone | 0.77 ± 0.20 | 0.76 ± 0.20 | 0.88 ± 0.06 | 0.92 ± 0.07 | 1.06 ± 0.03 |

**Table 5.** Biodistribution (%ID/g tissue) of [$^{18}$F]**5** in mice (Mean ± s.d., n = 3).

| Tissue | Time after injection | | | | |
|---|---|---|---|---|---|
| | 5 min | 15 min | 30 min | 60 min | 120 min |
| Blood | 1.10 ± 0.18 | 0.33 ± 0.03 | 0.21 ± 0.02 | 0.07 ± 0.01 | 0.14 ± 0.15 |
| Heart | 1.49 ± 0.21 | 0.48 ± 0.05 | 0.31 ± 0.04 | 0.08 ± 0.01 | 0.06 ± 0.01 |
| Lung | 1.55 ± 0.30 | 0.51 ± 0.04 | 0.33 ± 0.03 | 0.08 ± 0.01 | 0.06 ± 0.01 |
| Liver | 13.33 ± 0.14 | 5.45 ± 1.49 | 2.20 ± 0.22 | 0.57 ± 0.06 | 0.86 ± 0.08 |
| Pancreas | 1.74 ± 0.22 | 0.55 ± 0.04 | 0.35 ± 0.02 | 0.08 ± 0.01 | 0.05 ± 0.02 |
| Spleen | 0.97 ± 0.04 | 0.35 ± 0.01 | 0.20 ± 0.03 | 0.06 ± 0.01 | 0.04 ± 0.01 |
| Kidney | 2.73 ± 0.42 | 1.08 ± 0.08 | 0.62 ± 0.12 | 0.13 ± 0.02 | 0.09 ± 0.01 |
| Stomach | 2.60 ± 2.71 | 2.69 ± 2.28 | 5.18 ± 3.77 | 1.11 ± 0.50 | 3.03 ± 1.19 |
| S. Intestine | 43.83 ± 31.86 | 46.06 ± 12.57 | 18.45 ± 10.43 | 5.65 ± 2.22 | 10.60 ± 4.46 |
| L. Intestine | 1.08 ± 0.25 | 0.66 ± 0.39 | 0.28 ± 0.11 | 0.18 ± 0.06 | 0.73 ± 0.31 |
| Testis | 0.46 ± 0.05 | 0.30 ± 0.06 | 0.21 ± 0.08 | 0.10 ± 0.04 | 0.06 ± 0.03 |
| Muscle | 0.95 ± 0.16 | 0.41 ± 0.15 | 0.32 ± 0.12 | 0.08 ± 0.02 | 0.04 ± 0.01 |
| Brain | 0.54 ± 0.05 | 0.29 ± 0.02 | 0.26 ± 0.08 | 0.13 ± 0.02 | 0.08 ± 0.01 |
| Bone | 0.58 ± 0.09 | 0.19 ± 0.03 | 0.15 ± 0.02 | 0.07 ± 0.01 | 0.11 ± 0.00 |

To estimate the effective dose for standard human, we subsequently performed whole body dosimetry analyses using the biodistribution data from mice. The effective doses (mSv/MBq) in standard human were 0.013 for [$^{18}$F]**8**, 0.013 for [$^{18}$F]**9**, and 0.014 for [$^{18}$F]**5** (Supporting Information Table S2). The values were comparable to that reported for [$^{18}$F]FMeNER-$d_2$ (0.017 mSv/MBq),[61] a clinically used PET ligand for brain imaging. Although some defluorination of [$^{18}$F]**8** and [$^{18}$F]**9** was observed, their bone uptake was low (≈ 1%ID/g at 120 min after the injection). In fact, there was no difference in the effective dose among [$^{18}$F]**8**, [$^{18}$F]**9**, and [$^{18}$F]**5**.

**Metabolite Analysis in the Plasma and Brain**

Figure 5 shows the percentages of the unchanged forms of [$^{18}$F]**8**, [$^{18}$F]**9**, and [$^{18}$F]**5** in rat plasma (A) and brain (B). The respective fractions corresponding to the unchanged forms in plasma decreased from 25%–37% at 20 min to 21%–24% at 60 min after injection. Two polar radiolabeled metabolites [retention time ($t_R$) = 1.5–2.5 min] were observed for each radioligand on the plasma samples' HPLC charts (Supporting Information Figure S4). At 60 min after injection, the unchanged forms of [$^{18}$F]**8** and [$^{18}$F]**9** had retained 96% of total radioactivity in the brain, while the unchanged form of [$^{18}$F]**5** had retained 83% of total radioactivity in the brain. A certain level of the radiolabeled metabolite of [$^{18}$F]**5** in the brain was assumed to be [$^{18}$F]fluoroacetate, which might affect the quantitative analysis of PDE10A in brain. In contrast, [$^{18}$F]**8** and [$^{18}$F]**9** showed low levels of contamination by their radioactive metabolites in the brain, suggesting that their polar metabolites in plasma did not enter the brain easily and could not be converted to brain-permeable metabolites, such as [$^{18}$F]fluoroacetate. The extraction efficiency (Supporting Information Table S2) of metabolite analyses with [$^{18}$F]**8**, [$^{18}$F]**9**, or [$^{18}$F]**5** was obtained with over 84% in the brain at each time point, which strongly supported accuracy for this assessment.

The results of metabolite analyses indicate that [$^{18}$F]**8** and [$^{18}$F]**9** showed improved metabolism over [$^{18}$F]**5** in the brain. Considering that PET with [$^{18}$F]**9** produced the highest $BP_{ND}$ values among the newly developed radioligands and [$^{18}$F]**5**, we decide to proceed with [$^{18}$F]**9** for the further evaluations.

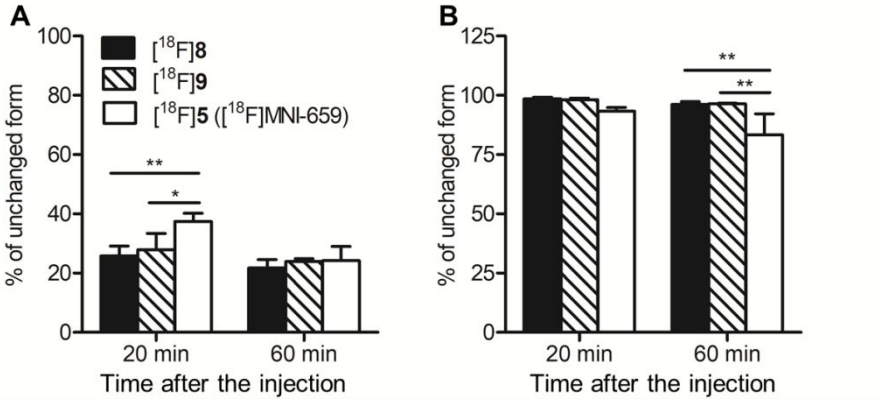


**Figure 5.** Percentages of unchanged forms of [$^{18}$F]**8**, [$^{18}$F]**9**, and [$^{18}$F]**5** in the plasma (A) and brain (B). **P < 0.01 (vs [$^{18}$F]**5**)

## CONCLUSION

In the present study, using [$^{18}$F]**5** as a lead compound, we developed four new PET radioligands [$^{18}$F]**6–9** for imaging of PDE10A and evaluated their in vitro and in vivo profiles using rodents. Of these PET ligands, two fluoromethoxy analogs ([$^{18}$F]**8** and [$^{18}$F]**9**) showed potent affinity for PDE10A and adequate lipophilicity. Furthermore, we found the highest in vivo availability ($BP_{ND}$) to PDE10A in the PET study with the

[$^{18}$F]fluoromethoxy-$d_2$ ligand [$^{18}$F]**9**, which showed low levels of contamination with its radiolabeled metabolites in the brain. Thus, [$^{18}$F]**9** may be a reasonable PET ligand for clinical studies of PDE10A imaging in human brains. We are planning to translate this radioligand for its first human study and then compare in vivo performance between [$^{18}$F]**5** and [$^{18}$F]**9** using head-to-head PET studies.

## EXPERIMENTAL SECTION

All chemical reagents and organic solvents were purchased from Sigma-Aldrich (St. Louis, MO, USA), FUJIFILM Wako Pure Chem. (Osaka, Japan), or Nacalai Tesque (Kyoto, Japan) and used without further purification. $^{18}$F was produced using a cyclotron (CYPRIS HM-18; Sumitomo Heavy Industries, Tokyo, Japan). Melting points (mp) were measured using a micro melting point apparatus (MP-500P, Yanaco; Tokyo, Japan) and were uncorrected. $^{1}$H NMR (300 MHz) spectra were recorded on a JEOL-AL-300 spectrometer (JEOL, Tokyo, Japan) using tetramethylsilane (TMS) as an internal standard. All chemical shifts (δ) are reported as ppm downfield relative to the TMS signal. Signals are quoted as s (singlet), d (doublet), t (triplet), br (broad), or m (multiplet). High-resolution fast atom bombardment mass spectra (HRMS) were acquired using a JEOL NMS-SX102 102A spectrometer. Silica gel column chromatography was performed

using Wakosil C-200 (FUJIFILM Wako Pure Chem.). HPLC separation and analysis were performed using a JASCO HPLC system (JASCO, Tokyo, Japan). All semi-preparative HPLC separations were performed using Capcell Pak $C_{18}$ columns (10 mm × 250 mm, Shiseido, Tokyo, Japan). All HPLC analyses were performed by using Capcell Pak $C_{18}$ columns (4.6 mm i.d. × 250 mm, Shiseido) to determine the chemical purities (>98%) of **6**–**9**. The analytic conditions were as follows: **6**: 1.0 mL/min, $CH_3CN/H_2O$ (75/25, v/v); **7**: 1.0 mL/min, $CH_3CN/H_2O/Et_3N$ (55/45/0.1, v/v/v); **8**: 1.0 mL/min, $CH_3CN/H_2O$ (65/35, v/v); **9**: 1.0 mL/min, $CH_3CN/H_2O$ (65/35, v/v). The radiochemical purities of [$^{18}$F]**6**–**9** were analyzed by the same HPLC and detector to monitor radioactivity under the following conditions: [$^{18}$F]**6**: 1.0 mL/min, $CH_3CN/H_2O$ (75/25, v/v); [$^{18}$F]**7**: 1.0 mL/min, $CH_3CN/H_2O/Et_3N$ (55/45/0.1,v/v/v); [$^{18}$F]**8**: 1.0 mL/min, $CH_3CN/H_2O$ (65/35, v/v); [$^{18}$F]**9**: 1.0 mL/min, $CH_3CN/H_2O$ (65/35, v/v). The authentic sample of **5** (MNI-659) was synthesized by reaction of **10** with 2-fluoroethyl-4-methylbenzenesulfonate. For the in vitro binding assay and preclinical evaluation, [$^{18}$F]**5** was synthesized by a reaction of **10** with [$^{18}$F]fluoroethyl bromide in house, as reported previously.[47]

**Chemical Synthesis**

**2-(2-(3-(4-(3-Fluoropropoxy)phenyl)-7-methyl-4-oxo-3,4-dihydroquinazolin-2-yl)ethyl)-4-isopropoxyisoindoline-1,3-dione (6).** A mixture of **10**[47] (150 mg, 0.31 mmol), **11** (79 mg, 0.34 mmol), and $K_2CO_3$ (64 mg, 0.46 mmol) in DMF (3 mL) was heated at 70° C for 11 h. After cooling, the reaction mixture was extracted with $CH_2Cl_2$, and the organic layer was washed with aqueous saturated $K_2CO_3$ solution, dried with $Na_2SO_4$, and evaporated under reduced pressure. Column chromatographic separation of the residue using hexane/ethyl acetate (AcOEt) (4/1, v/v) produced **6** (132 mg, 78%) as a white solid. mp: 161−163° C. $^1$H−NMR ($CDCl_3$): $\delta$ 1.38 (6H, d, $J$ = 6.3 Hz), 2.13–2.17 (1H, m), 2.21–2.26 (1H, m), 2.46 (3H, s), 2.73 (2H, t, $J$ = 6.9, 7.8 Hz), 4.07 (2H, t, $J$ = 7.2, 7.2 Hz), 4.14 (2H, t, $J$ = 6.0, 6.0 Hz), 4.58 (1H, t, $J$ = 5.7, 5.7 Hz), 4.66–4.76 (2H, m), 7.01 (2H, d, $J$ = 9.3 Hz), 7.14–7.22 (4H, m), 7.33 (1H, s), 7.36 (1H, d, $J$ = 7.5 Hz), 7.58 (1H, t, $J$ = 7.2, 8.4 Hz), 8.12 (1H, d, $J$ = 8.1 Hz). HRMS $m/z$: 544.4276 (calculated for $C_{31}H_{30}O_5N_3F$: 544.2248).

**2-(2-(3-(4-(3-Fluoro-2-hydroxypropoxy)phenyl)-7-methyl-4-oxo-3,4-dihydro-quinazolin-2-yl)ethyl)-4-isopropoxyisoindoline-1,3-dione (7).** A mixture of **10** (150 mg, 0.31 mmol), **12** (26 mg, 0.34 mmol), and $K_2CO_3$ (64 mg, 0.46 mmol) in DMF (3 mL) was heated at 80° C for 18 h. After cooling, the reaction mixture was extracted with

AcOEt and the organic layer was washed with brine, dried with $Na_2SO_4$, and evaporated under reduced pressure. Column chromatographic separation of the residue using hexane/AcOEt (1/1, v/v) produced **7** (52 mg, 30%) as a white solid. mp: 104–106° C. $^1$H−NMR (DMSO-$d_6$): $\delta$ 1.26 (6H, d, $J$ = 6.0 Hz), 2.41 (3H, s), 2.66 (2H, t, 2H, $J$ = 7.2, 7.2 Hz), 3.85 (2H, t, 2H, $J$ = 7.5, 6.9 Hz), 4.03–4.11 (3H, m), 4.39–4.47 (1H, m), 4.54–4.63 (1H, m), 4.73–4.81 (1H, m), 5.49 (1H, d, $J$ = 4.8 Hz), 7.10 (2H, d, $J$ = 8.4 Hz), 7.24 (1H, s), 7.30–7.44 (4H, m), 7.70 (1H, t, $J$ = 7.8, 7.8 HZ), 7.96 (2H, d, $J$ = 7.5 Hz). HRMS *m*/*z*: 560.2162 (calculated for $C_{31}H_{31}O_6N_3F$: 560.2197).

**2-(2-(3-(4-(Fluoromethoxy)phenyl)-7-methyl-4-oxo-3,4-dihydroquinazolin-2-yl)ethyl)-4-isopropoxyisoindoline-1,3-dione (8).** A mixture of **10** (80 mg, 0.17 mmol), **13** (37 mg, 0.18 mmol), and $K_2CO_3$ (34 mg, 0.25 mmol) in DMF (1.5 mL) was heated at 70° C for 18 h. After cooling, the reaction mixture was extracted with $CH_2Cl_2$, and the organic layer was washed with aqueous saturated $K_2CO_3$ solution, dried with $Na_2SO_4$, and evaporated under reduced pressure. Column chromatographic separation of the residue using hexane/AcOEt (3/2, v/v) produced **8** (23 mg, 27%) as a white solid. mp: 190–192° C. $^1$H−NMR ($CDCl_3$): $\delta$ 1.38 (6H, d, $J$ = 6.3 Hz), 2.47 (3H, s), 2.73 (2H, t, $J$ = 7.8, 6.9 Hz), 4.06 (2H, t, $J$ = 7.2, 7.5 Hz), 4.66–4.75 (1H, m), 5.68 (1H, s), 5.86 (1H, s),

7.17–7.37 (8H, m), 7.60 (1H, t, *J*=8.1, 7.8 Hz), 8.11 (1H, d, *J* = 8.1 Hz). HRMS *m*/*z*: 516.1937 (calculated for $C_{29}H_{26}O_5N_3F$: 516.1935).

**2-(2-(3-(4-(Fluoromethoxy-$d_2$)phenyl)-7-methyl-4-oxo-3,4-dihydroquinazolin-2-yl)ethyl)-4-isopropoxyisoindoline-1,3-dione (9).** A mixture of **10** (50 mg, 0.10 mmol), **16** (40 mg, 0.19 mmol), and $K_2CO_3$ (21 mg, 0.16 mmol) in DMF (2 mL) was heated at 70° C for 13 h. After cooling, the reaction mixture was extracted with $CH_2Cl_2$, and the organic layer was washed with aqueous saturated $K_2CO_3$ solution, dried with $Na_2SO_4$, and evaporated under reduced pressure. Column chromatographic separation of the residue using hexane/AcOEt (3/1, v/v) gave crude **9**, which was further purified using the semi-preparative HPLC column ($CH_3CN/H_2O$ = 65/35, 10 mL/min) to produce **9** (13.1 mg, 24%) as a white solid. mp: 193–195° C. $^1$H−NMR ($CDCl_3$): $\delta$ 1.38 (6H, d, *J* = 6.0 Hz), 2.47 (3H, s), 2.65 (2H, t, *J* = 7.8, 6.9 Hz), 4.05 (2H, t, *J* = 7.2, 7.5 Hz), 4.68–4.72 (1H, m), 7.13–7.38 (8H, m), 7.57–7.62 (1H, m), 8.10 (1H, d, *J* = 7.5 Hz). HRMS *m*/*z*: 518.2016 (calculated for $C_{29}H_{24}D_2O_5N_3F$: 516.1935).

**Methylene-$d_2$-bis(4-methylbenzenesulfonate) (15)**. A mixture of **14** (270 mg, 1 mmol) and silver *p*-toluenesulfonate (607 mg, 2.2 mmol) in $CH_3CN$ (2 mL) was heated at reflux

for 18 h. After cooling, the solvent was removed at reduced pressure. The residue was dissolved in warmed $CH_2Cl_2$ and filtered to remove the unreacted silver *p*-toluenesulfonate. The organic solvent was removed under reduced pressure, affording a crude product, which was recrystallized from ethanol to yield **15** (235 mg, 65%) as a white solid. mp: 109–111° C. $^1$H−NMR ($CDCl_3$): $\delta$ 2.45 (6H, s), 7.24 (4H, d, $J$ = 8.7 Hz), 7.59 (4H, d, $J$ = 8.1 Hz).

**Fluoromethyl-$d_2$-4-methylbenzenesulfonate (16).** A solution of **15** (228 mg, 0.64 mmol) in $CH_3CN$ (3 mL) was added to a solution of TBAF in THF (1 M, 1 mL, 1 mmol). Subsequently, the reaction mixture was heated at reflux for 26 h. The organic solvents were removed under reduced pressure, and the residue was extracted with AcOEt and water. The organic layer was washed with brine, dried over $MgSO_4$, and removed under reduced pressure. Column chromatographic separation of the residue using hexane/AcOEt (6/1, v/v) produced **12** (42 mg, 31%) as a colorless oil. $^1$H−NMR (300 MHz, $CDCl_3$): 2.46 (3H, s), 7.36 (2H, d, $J$ = 8.4 Hz), 7.83 (2H, d, $J$ = 8.4 Hz).

**Radiochemistry**

**2-(2-(3-(4-(3-[$^{18}$F]Fluoropropoxy)phenyl)-7-methyl-4-oxo-3,4-dihydroquinazolin-2-**

**yl)ethyl)-4-isopropoxyisoindoline-1,3-dione ([$^{18}$F]6).** [$^{18}$F]Hydrofluoride ([$^{18}$F]HF) was produced by the $^{18}$O(p, n)$^{18}$F reaction with 98 atom % $H_2{}^{18}O$ (Huayi Tech., Changsuo, China), and was separated from $H_2{}^{18}O$ using a Sep-Pak Accell Plus QMA Plus Light cartridge (Waters; Milford, MA). The produced [$^{18}$F]$F^-$ was eluted from the cartridge with a mixture of aqueous $K_2CO_3$ (4 mg/0.2 mL) and a solution of 4,7,13,16,21,24-hexaoxa-1,10-diazabicyclo[8,8,8]hexacosane (Kryptofix 222; 7.5 mg) in $CH_3CN$ (0.2 mL) and transferred into a reaction vessel in a hot cell. After the [$^{18}$F]KF solution was dried at 120° C for 30 min, a solution of **20** (20 μL) in *o*-dichlorobenzene (150 μL) was added to the reaction vial at 180° C. The resulting [$^{18}$F]**17** was distilled at 180° C under nitrogen and trapped in another reaction vial containing **10** (1.5 mg) and 0.5 M aqueous NaOH (6.2 μL) in anhydrous DMF (250 μL) at −15° C. After the radioactivity reached a plateau, which took 2.5 min, the reaction mixture was heated at 120° C for 10 min. The radioactive contents were diluted with 500 μL of HPLC mobile phase and transferred into the semi-preparative HPLC column. Elution with $CH_3CN/H_2O$ (70/30, v/v) at a flow rate of 5.0 mL/min gave a radioactive fraction corresponding to pure [$^{18}$F]**6** ($t_R$: 9.6 min). The HPLC fractions of [$^{18}$F]**6** were collected into a flask to which Tween 80 (75 μL) in ethanol (300 μL) and 25% ascorbic acid (0.1 mL) had been added before radiosynthesis. The fractions were subsequently evaporated to dryness under reduced pressure, and the residue was

dissolved in physiological saline (3 mL) to obtain [$^{18}$F]**6** as an injectable solution. The identity of [$^{18}$F]**6** ($t_R$: 6.5 min) was confirmed by analytical HPLC with **6**. The result of a typical batch was as follows: synthesis time from end of bombardment (EOB), 64 min; radiochemical yield (decay-corrected based on [$^{18}$F]$F^-$), 7%; radiochemical purity, >99%; molar activity at EOS, 168 GBq/μmol.

**2-(2-(3-(4-(3-[$^{18}$F]Fluoro-2-hydroxypropoxy)phenyl)-7-methyl-4-oxo-3,4-dihydroquinazolin-2-yl)ethyl)-4-isopropoxyisoindoline-1,3-dione ([$^{18}$F]7).** After the [$^{18}$F]$F^-$ solution was dried at 120° C for 30 min, a solution of **21** (20 μL) in *o*-dichlorobenzene (150 μL) was added to the reaction vial containing dry [$^{18}$F]$F^-$ at 180° C. The produced [$^{18}$F]**12** was distilled and trapped into a solution of **10** (2.0 mg) and 1.0 M aqueous NaOH (4.1 μL) in anhydrous DMF (250 μL) at −15° C. After the radioactivity reached a plateau, which took 2 min, the reaction mixture was heated at 130° C for 20 min. HPLC separation was completed using a mobile phase of $CH_3CN/H_2O/Et_3N$ (55/45/0.1, v/v/v) at a flow rate of 5.0 mL/min. The HPLC fractions of [$^{18}$F]**7** ($t_R$ = 12.6 min) were collected and then treated to obtain [$^{18}$F]**7** as an injectable solution. The identity of [$^{18}$F]**7** ($t_R$: 10.7 min) was confirmed by analytical HPLC with **7**. The result of a typical batch was as follows: synthesis time from EOB, 74 min; radiochemical yield (decay-

corrected based on [$^{18}$F]F$^-$), 2%; radiochemical purity, >99%; molar activity at EOS, 262 GBq/μmol.

**2-(2-(3-(4-([$^{18}$F]Fluoromethoxy)phenyl)-7-methyl-4-oxo-3,4-dihydroquinazolin-2-yl)ethyl)-4-isopropoxyisoindoline-1,3-dione ([$^{18}$F]8).** After the [$^{18}$F]F$^-$ solution was dried at 120° C for 30 min, a solution of **22** (10 μL) in $CH_3CN$ (150 μL) was added to the reaction vial. The mixture was heated for 5 min at 100° C. The resulting [$^{18}$F]**18** was distilled at 30° C, passed through 3 silica Sep-Pak columns (Waters) linked in series for 6.5 min using nitrogen gas, and trapped into a solution of **10** (1.0 mg) and 0.5 M aqueous NaOH (4.2 μL) in anhydrous DMF (300 μL) at −15° C. After the radioactivity reached a plateau, which took 6 min, the reaction mixture was heated at 90° C for 5 min. HPLC separation was completed using a mobile phase of $CH_3CN/H_2O$ (65/35, v/v) at a flow rate of 5.0 mL/min. The HPLC fractions of [$^{18}$F]**8** ($t_R$ = 10 min) were collected and treated to obtain [$^{18}$F]**8** as an injectable solution. The identity of [$^{18}$F]**8** ($t_R$: 9.4 min) was confirmed by analytical HPLC with **8**. The result of a typical batch was as follows: synthesis time from EOB, 56 min; radiochemical yield (decay-corrected based on [$^{18}$F]F$^-$), 9%; radiochemical purity, >99%; molar activity at EOS, 336 GBq/μmol.

**2-(2-(3-(4-([$^{18}$F]Fluoromethoxy-$d_2$)phenyl)-7-methyl-4-oxo-3,4-dihydroquinazolin-2-yl)ethyl)-4-isopropoxyisoindoline-1,3-dione ([$^{18}$F]9).** After the [$^{18}$F]$F^-$ solution was dried at 120° C for 30 min, a solution of **23** (10 μL) in $CH_3CN$ (150 μL) was added to the reaction vial. The mixture was heated for 5 min at 100° C. The resulting [$^{18}$F]**19** was distilled at 30° C, passed through 3 silica Sep-Pak columns linked in series, and trapped into a solution of **10** (1.0 mg) and 0.5 M NaOH aq (4.2 μL) in anhydrous DMF (300 μL) at −15° C. After the radioactivity reached a plateau, which took 6.5 min, the reaction mixture was heated at 90° C for 5 min. HPLC separation was completed using a mobile phase of $CH_3CN/H_2O$ (65/35, v/v) at a flow rate of 5.0 mL/min. The HPLC fractions of [$^{18}$F]**9** ($t_R$ = 10.2 min) were collected and treated to obtain [$^{18}$F]**9** as an injectable solution. The identity of [$^{18}$F]**9** ($t_R$: 9.7 min) was confirmed by analytical HPLC with **9**. The result of a typical batch was as follows: synthesis time from EOB, 59 min; radiochemical yield (decay-corrected based on [$^{18}$F]$F^-$), 10%; radiochemical purity, >99%; molar activity at EOS, 293 GBq/μmol.

**Measurement of Lipophilicity.** The LogD value was measured by mixing [$^{18}$F]**5**–**9** with *n*-octanol (3.0 g) and phosphate buffered saline (PBS; 3.0 g, 0.1 M, pH 7.4) in a test tube, which was vortexed for 3 min at room temperature followed by centrifugation at 3500 *g*

for 5 min. An aliquot of 0.65 mL PBS and 0.65 mL *n*-octanol was removed and weighed, and its radioactivity was counted with an autogamma counter (2480 Wizard$^2$, Perkin-Elmer, Waltham, MA). Each sample from the remaining organic layer was removed and repartitioned until a consistent LogD value was obtained. The LogD value was calculated by comparing the ratio of counts per minute (cpm)/g of *n*-octanol to that of PBS and is expressed as LogD = Log[cpm/g (*n*-octanol)/cpm/g (PBS)]. All measurements were performed in triplicate.

**Animals.** Male Sprague-Dawley (SD) rats and ddY mice were purchased from Japan SLC (Shizuoka, Japan), kept in a temperature-controlled environment with a 12-h light/dark cycle, and fed a standard diet (MB-1/Funabashi Farm, Chiba, Japan). Animal experiments were performed according to the recommendations of the Committee for the Care and Use of Laboratory Animals in QST and the ARRIVE guidelines (http://www.nc3rs.org/ARRIVE).

**In vitro Binding Assay.** Two SD rats were killed by decapitation under anesthesia (3% isoflurane in air). The brains, except the cerebellum, were rapidly removed and homogenized with a Silent Crusher S homogenizer (Heidolph Instruments, Schwabach,

Germany) in 10 volumes of 50 mM Tris-HCl (pH 7.4) containing 120 mM NaCl. After the homogenate was centrifuged at 300 *g* for 15 min at 4° C, the supernatant was stored at −80° C before use.

The supernatant of the brain homogenate was diluted to 50 mg tissue/mL in 50 mM Tris-HCl buffer containing 120 mM NaCl, 2 mM KCl, 1 mM $MgCl_2$, and 1 mM $CaCl_2$. Each preparation of 0.1 mL brain tissue solution was incubated with [$^{18}$F]**5** (0.2–0.4 nM in buffer) and 0.1 mL of test compounds **5**–**9** ($10^{-1}$–$10^{2}$ nM in 0.1–1% DMSO) in a final volume of 1 mL buffer. These mixtures were incubated for 30 min at room temperature. The bound and free radioligands were separated by vacuum filtration through 0.3% polyethylenimine-pretreated Whatman GF/C glass fiber filters using a cell harvester (M-24, Brandel, Gaithersburg, MD) followed by three washes with prechilled tris-buffer. The radioactivity of washed filters containing the specifically bound [$^{18}$F]**5** was measured by an autogamma scintillation counter (2480 Wizard$^2$). In the present study, the dissociation constant ($K_D$) of [$^{18}$F]**5** from PDE10A in the brain tissue was determined using GraphPad Prism 5 (GraphPad Software, La Jolla, CA) (Supporting Information Figure S5). The results of the inhibitory experiments were subjected to nonlinear regression analysis, in which the inhibition constant ($K_i$) was calculated.

**Small-Animal PET Studies.** Each rat was anesthetized with 1.5% (v/v) isoflurane, and a 24-gauge intravenous catheter (Terumo Medical Products, Tokyo) was inserted into the tail vein. Rats were subsequently maintained under anesthesia and secured in a custom-designed chamber placed in the center of a small-animal PET scanner (Inveon; Siemens Medical Solutions, Knoxville, TN).

After target position adjustment for brain scanning, [$^{18}$F]**6** (n = 1, 10 MBq, 59 fmol), [$^{18}$F]**7** (n = 1, 11 MBq, 41 fmol), [$^{18}$F]**8** (n = 3, 11–13 MBq, 67–82 fmol), [$^{18}$F]**9** (n = 5, 11–15 MBq, 40–65 fmol), and [$^{18}$F]**5** (n = 4, 13–16 MBq, 65–67 fmol) were respectively injected via the tail vein catheter, and then dynamic emission scans were conducted for 60 min (10 s × 12 frames, 20 s × 3 frames, 30 s × 3 frames, 1 min × 3 frames, 2.5 min × 3 frames, and 5 min × 9 frames) (in three-dimensional list mode). Rat body temperatures were maintained at 37° C using a heated water circulation system (T/Pump TP401; Gaymar Industries, Orchard Park, NY) during the PET scans.

For blocking study, two rats were administrated with unlabeled **5** (MNI-659 dissolved in DMSO) of 5 mg/kg 20 min after the injection of [$^{18}$F]**9** (n = 2, 14–15 MBq, 94–95 fmol) or [$^{18}$F]**5** (n = 2, 13–15 MBq, 61–71 fmol).

**Data Analysis.** The PET dynamic image data with 0.6-mm slice thickness were

reconstructed by filtered back-projection using a Hanning filter with a Nyquist cutoff of 0.5 cycles per pixel. Averaged summation PET images were produced and fused with a magnetic resonance imaging (MRI) template using the PMOD software package (version 3.4; PMOD technology, Zurich, Switzerland). To obtain $BP_{ND}$ for PDE10A as a quantitative index of specific radioligand binding, tTAC for each radioligand was acquired from the volumes of interest, which were anatomically drawn onto the striatum (PDE10A-rich region) and midbrain (poor region) based on a rat brain MRI template. The radioactivity was decay-corrected to the injection time and expressed as the standardized uptake value (SUV), which was normalized to the injected radioactivity and body weight. SUV was calculated according to the following formula: SUV = (radioactivity per mL tissue/injected radioactivity) × grams body weight. The kinetic analysis for estimation of the $BP_{ND}$ value of each radioligand was performed with SRTM[57,60] using tTACs obtained from the midbrain as the reference region.

**Biodistribution Study in Mice**. Each mouse (36–41 g) was injected with a bolus of the radioligand ([$^{18}$F]**8**: 2.5 MBq/0.1 mL, 17.2 fmol; [$^{18}$F]**9**: 1.3 MBq/0.1 mL, 9.9 fmol; [$^{18}$F]**5**: 1.9 MBq/0.1 mL, 3.9 fmol) via the tail vein. Three mice were sacrificed at each experimental time point (5, 15, 30, 60, and 120 min) after the injection by cervical

dislocation. The whole brain, heart, liver, lung, spleen, testis, kidney, pancreas, stomach (including contents), small intestines (including contents), large intestines (including contents), muscle, thigh bone, and blood samples were removed quickly. The radioactivity in these tissues was measured with an autogamma scintillation counter (2480 Wizard$^2$) and expressed as %ID/g. All radioactivity measurements were corrected for decay.

To estimate the organ-absorbed and effective doses, we extrapolated the data from mice to standard human using OLINDA EXM (version 1.1, Vanderbilt University, Nashville, TN).[62]

**Metabolite Analysis of the Plasma and Brain**. Following the intravenous injection of each radioligand ([$^{18}$F]**8**: 30 MBq, 0.2 mL, 0.2-pmol; [$^{18}$F]**9**: 30 MBq, 0.2 mL, 0.2 pmol; [$^{18}$F]**5**: 30 MBq, 0.15 mL, 0.2 pmol), the rats (n = 3 for each time point) were sacrificed by cervical dislocation at 20, and 60 min. Blood and brain samples were quickly removed. The blood samples were centrifuged at 15,000 *g* for 2 min at 4° C to separate the plasma. The plasma (0.3 mL) was collected in a test tube containing $CH_3CN$ (0.3 mL), and the resulting mixture was vortexed for 15 s and then centrifuged at 15,000 *g* for 2 min for deproteinization. The resulting supernatant was collected and then the pellet was

resuspended using $CH_3CN$ (0.2 mL). Subsequently, the mixture was centrifuged at 15,000 *g* for 2 min. The supernatant was collected. The brain samples excepting cerebellum were homogenized using a homogenizer (Silent Crusher S; Heidolph, Schwabach, Germany) in ice-cooled saline (2.0 mL). The resulting homogenate (0.5 mL) was added into a test tube containing $CH_3CN$ (0.5 mL), vortexed, and centrifuged at 15,000 *g* for 2 min at 4° C. After the supernatant was collected, the pellet was resuspended with $CH_3OH$ (0.3 mL) and then centrifuged at 15,000 *g* for 2 min. The resulting supernatant was collected. Subsequently, an aliquot of the supernatant (0.2–0.3 mL) obtained from the plasma or brain homogenate was injected into the HPLC system with a radioactivity detector and analyzed using a Capcell Pak $C_{18}$ column with a mobile phase ($CH_3CN/H_2O$ = 70/30, v/v) at a flow rate of 1.5 mL/min. The percent ratio of the unchanged form to total radioactivity (corrected for decay) on the HPLC chromatograms was calculated as % = (peak area of [$^{18}$F]ligand / total peak area) × 100. The extraction efficiency of [$^{18}$F]**8**, [$^{18}$F]**9**, and [$^{18}$F]**5** was confirmed by counting radioactivity in each pellet and supernatant after the deproteinization of plasma and brain at each time point using an autogamma scintillation counter (2480 Wizard[2]).

**Statistics**. All data are expressed as mean ± standard deviation (s.d.). The differences

between each radioligand were calculated using one- or two-way repeated measures analyses of variance. Post hoc analyses employed the Bonferroni method. Statistical significance (denoted with asterisks in the figures and table) was determined at a 95% confidence level ($P < 0.05$). All statistical data were analyzed using GraphPad Prism 5.

## ASSOCIATED CONTENT

### Supporting Information

Purities of **5**–**10** determined by HPLC; HPLC analytic charts of **5**–**10**; HPLC purification charts of [$^{18}$F]**5**–**9**; HPLC analytical charts of [$^{18}$F]**5**–**9**; Estimated effective doses of [$^{18}$F]**8,** [$^{18}$F]**9**, and [$^{18}$F]**5** in standard human; Representative radio-HPLC charts in metabolite analyses of [$^{18}$F]**8**, [$^{18}$F]**9**, and [$^{18}$F]**5**; and Determination of $K_D$ value of [$^{18}$F]**5** for PDE10A.

## AUTHOR INFORMATION

### Corresponding Author

Ming-Rong Zhang, PhD., Department of Radiopharmaceuticals Development, National Institute of Radiological Sciences, National Institutes for Quantum and Radiological Science and Technology, 4-9-1 Anagawa, Inage-ku, Chiba 263-8555, Japan. Phone: 81-43-382-3709; fax: 81-43-206-3261; e-mail: zhang.ming-rong@qst.go.jp.

## Author Contributions

[I]W.M. and T.Y. contributed equally.

## Notes

The authors declare no competing financial interests.

## ACKNOWLEDGMENTS

We thank the staff of the National Institutes for Quantum and Radiological Sciences and Technology (QST) for their support with cyclotron operation, radioisotope production, radiosynthesis, and animal experiments. This study was supported in part by a Grant-in-Aid for Scientific Research (Basic Research B: 17H04267) from the Ministry of Education, Culture, Sports, Science and Technology of the Japanese Government.

## ABBREVIATIONS USED

$BP_{ND}$, nondisplaceable binding potential; DMF, *N*,*N*-dimethylformamide; DMSO, dimethyl sulfoxide; EOB, end of bombardment; EOS, end of synthesis; %ID/g, percentage of the injected dose per gram of wet tissue; $K_i$, binding affinity; PET, positron emission tomography; SRTM, simplified reference tissue model; SD, Sprague-Dawley; SUV, standardized uptake value; tTAC, tissue time–activity curve; $t_R$, retention time.

## REFERENCES

1. Soderling, S. H.; Beavo, J. A., Regulation of cAMP and cGMP signaling: new phosphodiesterases and new functions. *Current opinion in cell biology*. **2000,** *12*, 174–179.

2. Conti, M.; Beavo, J., Biochemistry and physiology of cyclic nucleotide phosphodiesterases: essential components in cyclic nucleotide signaling. *Annu. Rev. Biochem.* **2007,** *76*, 481–511.

3. Francis, S. H.; Blount, M. A.; Corbin, J. D., Mammalian cyclic nucleotide phosphodiesterases: molecular mechanisms and physiological functions. *Physiol. Rev.* **2011,** *91*, 651–690.

4. Wood, E. R.; Bledsoe, R.; Chai, J.; Daka, P.; Deng, H.; Ding, Y.; Harris-Gurley, S.; Kryn, L. H.; Nartey, E.; Nichols, J.; Nolte, R. T.; Prabhu, N.; Rise, C.; Sheahan, T.; Shotwell, J. B.; Smith, D.; Tai, V.; Taylor, J. D.; Tomberlin, G.; Wang, L.; Wisely, B.; You, S.; Xia, B.; Dickson, H., The role of phosphodiesterase 12 (PDE12) as a negative regulator of the innate immune response and the discovery of antiviral inhibitors. *J. Biol. Chem.* **2015,** *290*, 19681–19696.

5. Xie, Z.; Adamowicz, W. O.; Eldred, W. D.; Jakowski, A. B.; Kleiman, R. J.; Morton, D. G.; Stephenson, D. T.; Strick, C. A.; Williams, R. D.; Menniti, F. S., Cellular and subcellular localization of PDE10A, a striatum-enriched phosphodiesterase. *Neuroscience.* **2006,** *139*, 597–607.

6. Lakics, V.; Karran, E. H.; Boess, F. G., Quantitative comparison of phosphodiesterase mRNA distribution in human brain and peripheral tissues. *Neuropharmacology.* **2010,** *59*, 367–374.

7. Chappie, T. A.; Helal, C. J.; Hou, X., Current landscape of phosphodiesterase

10A (PDE10A) inhibition. *J. Med. Chem.* **2012,** *55*, 7299–7331.

8. Kehler, J.; Nielsen, J., PDE10A inhibitors: novel therapeutic drugs for schizophrenia. *Curr. Pharm. Des.* **2011,** *17*, 137–150.

9. Harada, A.; Suzuki, K.; Kimura, H., TAK-063, a novel phosphodiesterase 10A inhibitor, protects from striatal neurodegeneration and ameliorates behavioral deficits in the R6/2 mouse model of Huntington's disease. *J. Pharmacol. Exp. Ther.* **2017,** *360*, 75–83.

10. Shiraishi, E.; Suzuki, K.; Harada, A.; Suzuki, N.; Kimura, H., The phosphodiesterase 10A selective inhibitor TAK-063 improves cognitive functions associated with Schizophrenia in rodent models. *J. Pharmacol. Exp. Ther.* **2016,** *356*, 587–595.

11. Suzuki, K.; Harada, A.; Suzuki, H.; Miyamoto, M.; Kimura, H., TAK-063, a PDE10A inhibitor with balanced activation of direct and indirect pathways, provides potent antipsychotic-like effects in multiple paradigms. *Neuropsychopharmacology.* **2016,** *41*, 2252–2262.

12. Niccolini, F.; Foltynie, T.; Reis Marques, T.; Muhlert, N.; Tziortzi, A. C.; Searle, G. E.; Natesan, S.; Kapur, S.; Rabiner, E. A.; Gunn, R. N.; Piccini, P.; Politis, M., Loss of phosphodiesterase 10A expression is associated with progression and severity in Parkinson's disease. *Brain.* **2015,** *138*, 3003–3015.

13. Celen, S.; Koole, M.; De Angelis, M.; Sannen, I.; Chitneni, S. K.; Alcazar, J.; Dedeurwaerdere, S.; Moechars, D.; Schmidt, M.; Verbruggen, A.; Langlois, X.; Van Laere, K.; Andres, J. I.; Bormans, G., Preclinical evaluation of $^{18}$F-JNJ41510417 as a radioligand for PET imaging of phosphodiesterase-10A in the brain. *J. Nucl. Med.* **2010,** *51*, 1584–1591.

14. Tu, Z.; Fan, J.; Li, S.; Jones, L. A.; Cui, J.; Padakanti, P. K.; Xu, J.; Zeng, D.; Shoghi, K. I.; Perlmutter, J. S.; Mach, R. H., Radiosynthesis and in vivo evaluation of [$^{11}$C]MP-10 as a PET probe for imaging PDE10A in rodent and non-human primate brain. *Bioorg. Med. Chem.* **2011,** *19*, 1666–1673.

15. Andres, J. I.; De Angelis, M.; Alcazar, J.; Iturrino, L.; Langlois, X.; Dedeurwaerdere, S.; Lenaerts, I.; Vanhoof, G.; Celen, S.; Bormans, G., Synthesis, in vivo occupancy, and radiolabeling of potent phosphodiesterase subtype-10 inhibitors as candidates for positron emission tomography imaging. *J. Med. Chem.* **2011,** *54*, 5820–5835.

16. Tu, Z.; Xu, J.; Jones, L. A.; Li, S.; Mach, R. H., Carbon-11 labeled papaverine as a PET tracer for imaging PDE10A: radiosynthesis, in vitro and in vivo evaluation. *Nucl. Med. Biol.* **2010,** *37*, 509–516.

17. Hwang, D. R.; Hu, E.; Rumfelt, S.; Easwaramoorthy, B.; Castrillon, J.; Davis, C.; Allen, J. R.; Chen, H.; Treanor, J.; Abi-Dargham, A.; Slifstein, M., Initial characterization of a PDE10A selective positron emission tomography tracer [$^{11}$C]AMG 7980 in non-human primates. *Nucl. Med. Biol.* **2014,** *41*, 343–349.

18. Fan, J.; Zhang, X.; Li, J.; Jin, H.; Padakanti, P. K.; Jones, L. A.; Flores, H. P.; Su, Y.; Perlmutter, J. S.; Tu, Z., Radiosyntheses and in vivo evaluation of carbon-11 PET tracers for PDE10A in the brain of rodent and nonhuman primate. *Bioorg. Med. Chem.* **2014,** *22*, 2648–2654.

19. Barret, O.; Thomae, D.; Tavares, A.; Alagille, D.; Papin, C.; Waterhouse, R.; McCarthy, T.; Jennings, D.; Marek, K.; Russell, D.; Seibyl, J.; Tamagnan, G., In vivo assessment and dosimetry of 2 novel PDE10A PET radiotracers in humans: $^{18}$F-MNI-659 and $^{18}$F-MNI-654. *J. Nucl. Med.* **2014,** *55*, 1297–1304.

20. Kehler, J.; Kilburn, J. P.; Estrada, S.; Christensen, S. R.; Wall, A.; Thibblin, A.; Lubberink, M.; Bundgaard, C.; Brennum, L. T.; Steiniger-Brach, B.; Christoffersen, C. T.; Timmermann, S.; Kreilgaard, M.; Antoni, G.; Bang-Andersen, B.; Nielsen, J., Discovery and development of $^{11}$C-Lu AE92686 as a radioligand for PET imaging of phosphodiesterase10A in the brain. *J. Nucl. Med.* **2014,** *55*, 1513–1518.

21. Ooms, M.; Celen, S.; Koole, M.; Langlois, X.; Schmidt, M.; De Angelis, M.; Andres, J. I.; Verbruggen, A.; Van Laere, K.; Bormans, G., Synthesis and biological evaluation of carbon-11 and fluorine-18 labeled tracers for in vivo visualization of PDE10A. *Nucl. Med. Biol.* **2014,** *41*, 695–704.

22. Harada, A.; Suzuki, K.; Miura, S.; Hasui, T.; Kamiguchi, N.; Ishii, T.; Taniguchi, T.; Kuroita, T.; Takano, A.; Stepanov, V.; Halldin, C.; Kimura, H., Characterization of the binding properties of T-773 as a PET radioligand for phosphodiesterase 10A. *Nucl. Med. Biol.* **2015,** *42* (2), 146–154.

23. Yang, H.; Murigi, F. N.; Wang, Z.; Li, J.; Jin, H.; Tu, Z., Synthesis and in vitro characterization of cinnoline and benzimidazole analogues as phosphodiesterase 10A inhibitors. *Bioorg. Med. Chem. Lett.* **2015,** *25*, 919–924.

24. Stepanov, V.; Miura, S.; Takano, A.; Amini, N.; Nakao, R.; Hasui, T.; Nakashima, K.; Taniguchi, T.; Kimura, H.; Kuroita, T.; Halldin, C., Development of a series of novel carbon-11 labeled PDE10A inhibitors. *J. Labelled. Comp. Radiopharm.* **2015,** *58*, 202–208.

25. Hwang, D. R.; Hu, E.; Allen, J. R.; Davis, C.; Treanor, J.; Miller, S.; Chen, H.; Shi, B.; Narayanan, T. K.; Barret, O.; Alagille, D.; Yu, Z.; Slifstein, M., Radiosynthesis and initial characterization of a PDE10A specific PET tracer [$^{18}$F]AMG 580 in non-human primates. *Nucl. Med. Biol.* **2015,** *42*, 654–663.

26. Cox, C. D.; Hostetler, E. D.; Flores, B. A.; Evelhoch, J. L.; Fan, H.; Gantert, L.; Holahan, M.; Eng, W.; Joshi, A.; McGaughey, G.; Meng, X.; Purcell, M.; Raheem, I. T.; Riffel, K.; Yan, Y.; Renger, J. J.; Smith, S. M.; Coleman, P. J., Discovery of [$^{11}$C]MK-8193 as a PET tracer to measure target engagement of phosphodiesterase 10A (PDE10A) inhibitors. *Bioorg. Med. Chem. Lett.* **2015,** *25*, 4893–4898.

27. Li, J.; Zhang, X.; Jin, H.; Fan, J.; Flores, H.; Perlmutter, J. S.; Tu, Z., Synthesis of fluorine-containing phosphodiesterase 10A (PDE10A) inhibitors and the in vivo evaluation of F-18 labeled PDE10A PET tracers in rodent and nonhuman primate. *J. Med. Chem.* **2015,** *58*, 8584–8600.

28. Wagner, S.; Teodoro, R.; Deuther-Conrad, W.; Kranz, M.; Scheunemann, M.; Fischer, S.; Wenzel, B.; Egerland, U.; Hoefgen, N.; Steinbach, J.; Brust, P., Radiosynthesis and biological evaluation of the new PDE10A radioligand [$^{18}$F]AQ28A. *J. Labelled. Comp. Radiopharm.* **2017,** *60*, 36–48.

29. Stepanov, V.; Takano, A.; Nakao, R.; Amini, N.; Miura, S.; Hasui, T.; Kimura, H.; Taniguchi, T.; Halldin, C., Development of two fluorine-18 labeled PET radioligands targeting PDE10A and in vivo PET evaluation in nonhuman primates. *Nucl. Med. Biol.* **2018,** *57*, 12–19.

30. Takano, A.; Stenkrona, P.; Stepanov, V.; Amini, N.; Martinsson, S.; Tsai, M.; Goldsmith, P.; Xie, J.; Wu, J.; Uz, T.; Halldin, C.; Macek, T. A., A human [$^{11}$C]T-773 PET study of PDE10A binding after oral administration of TAK-063, a PDE10A inhibitor. *Neuroimage.* **2016,** *141*, 10–17.

31. Boden, R.; Persson, J.; Wall, A.; Lubberink, M.; Ekselius, L.; Larsson, E. M.; Antoni, G., Striatal phosphodiesterase 10A and medial prefrontal cortical thickness in patients with schizophrenia: a PET and MRI study. *Transl. Psychiatry.* **2017,** *7*, e1050.

32. Plisson, C.; Weinzimmer, D.; Jakobsen, S.; Natesan, S.; Salinas, C.; Lin, S. F.; Labaree, D.; Zheng, M. Q.; Nabulsi, N.; Marques, T. R.; Kapur, S.; Kawanishi, E.; Saijo, T.; Gunn, R. N.; Carson, R. E.; Rabiner, E. A., Phosphodiesterase 10A PET radioligand development program: from pig to human. *J. Nucl. Med.* **2014,** *55*, 595–601.

33. Niccolini, F.; Haider, S.; Reis Marques, T.; Muhlert, N.; Tziortzi, A. C.; Searle, G. E.; Natesan, S.; Piccini, P.; Kapur, S.; Rabiner, E. A.; Gunn, R. N.; Tabrizi, S. J.; Politis, M., Altered PDE10A expression detectable early before symptomatic onset in Huntington's disease. *Brain.* **2015,** *138*, 3016–3029.

34. Marques, T. R.; Natesan, S.; Niccolini, F.; Politis, M.; Gunn, R. N.; Searle, G. E.; Howes, O.; Rabiner, E. A.; Kapur, S., Phosphodiesterase 10A in Schizophrenia: A PET study using [$^{11}$C]IMA107. *Am. J. Psychiatry.* **2016,** *173*, 714–721.

35. Wilson, H.; Niccolini, F.; Haider, S.; Marques, T. R.; Pagano, G.; Coello, C.; Natesan, S.; Kapur, S.; Rabiner, E. A.; Gunn, R. N.; Tabrizi, S. J.; Politis, M., Loss of extra-striatal phosphodiesterase 10A expression in early premanifest Huntington's disease gene carriers. *J. Neurol. Sci.* **2016,** *368*, 243–248.

36. Van Laere, K.; Ahmad, R. U.; Hudyana, H.; Celen, S.; Dubois, K.; Schmidt, M. E.; Bormans, G.; Koole, M., Human biodistribution and dosimetry of $^{18}$F-JNJ42259152, a radioligand for phosphodiesterase 10A imaging. *Eur. J. Nucl. Med. Mol. Imaging.* **2013,** *40*, 254–261.

37. Van Laere, K.; Ahmad, R. U.; Hudyana, H.; Dubois, K.; Schmidt, M. E.; Celen, S.; Bormans, G.; Koole, M., Quantification of $^{18}$F-JNJ-42259152, a novel phosphodiesterase 10A PET tracer: kinetic modeling and test-retest study in human brain. *J. Nucl. Med.* **2013,** *54*, 1285–1293.

38. Russell, D. S.; Jennings, D. L.; Barret, O.; Tamagnan, G. D.; Carroll, V. M.;

Caille, F.; Alagille, D.; Morley, T. J.; Papin, C.; Seibyl, J. P.; Marek, K. L., Change in PDE10 across early Huntington disease assessed by [$^{18}$F]MNI-659 and PET imaging. *Neurology.* **2016,** *86* (8), 748–754.

39. Delnomdedieu, M.; Forsberg, A.; Ogden, A.; Fazio, P.; Yu, C. R.; Stenkrona, P.; Duvvuri, S.; David, W.; Al-Tawil, N.; Vitolo, O. V.; Amini, N.; Nag, S.; Halldin, C.; Varrone, A., In vivo measurement of PDE10A enzyme occupancy by positron emission tomography (PET) following single oral dose administration of PF-02545920 in healthy male subjects. *Neuropharmacology.* **2017,** *117*, 171–181.

40. Fazio, P.; Schain, M.; Mrzljak, L.; Amini, N.; Nag, S.; Al-Tawil, N.; Fitzer-Attas, C. J.; Bronzova, J.; Landwehrmeyer, B.; Sampaio, C.; Halldin, C.; Varrone, A., Patterns of age related changes for phosphodiesterase type-10A in comparison with dopamine D2/3 receptors and sub-cortical volumes in the human basal ganglia: A PET study with $^{18}$F-MNI-659 and $^{11}$C-raclopride with correction for partial volume effect. *Neuroimage.* **2017,** *152*, 330–339.

41. Schain, M.; Fazio, P.; Mrzljak, L.; Amini, N.; Al-Tawil, N.; Fitzer-Attas, C.; Bronzova, J.; Landwehrmeyer, B.; Sampaio, C.; Halldin, C.; Varrone, A., Revisiting the Logan plot to account for non-negligible blood volume in brain tissue. *EJNMMI. Res.* **2017,** *7*, 66.

42. Liu, H.; Jin, H.; Yue, X.; Han, J.; Yang, H.; Flores, H.; Su, Y.; Alagille, D.; Perlmutter, J. S.; Tamagnan, G.; Tu, Z., Comparison of [$^{11}$C]TZ1964B and [$^{18}$F]MNI659 for PET imaging brain PDE10A in nonhuman primates. *Pharmacol. Res. Perspect.* **2016,** *4*, e00253.

43. Eberl, S.; Katsifis, A.; Peyronneau, M. A.; Wen, L.; Henderson, D.; Loc'h, C.; Greguric, I.; Verschuer, J.; Pham, T.; Lam, P.; Mattner, F.; Mohamed, A.; Fulham, M. J.,

Preclinical in vivo and in vitro comparison of the translocator protein PET ligands [$^{18}$F]PBR102 and [$^{18}$F]PBR111. *Eur. J. Nucl. Med. Mol. Imaging.* **2017,** *44*, 296–307.

44. Fonnum, F.; Johnsen, A.; Hassel, B., Use of fluorocitrate and fluoroacetate in the study of brain metabolism. *Glia.* **1997,** *21*, 106–113.

45. Yamauchi, H.; Kagawa, S.; Kishibe, Y.; Takahashi, M.; Nishii, R.; Mizuma, H.; Takahashi, K.; Onoe, H.; Higashi, T., Increase in [$^{18}$F]fluoroacetate uptake in patients with chronic hemodynamic cerebral ischemia. *Stroke.* **2015,** *46*, 2669–2672.

46. Ponde, D. E.; Dence, C. S.; Oyama, N.; Kim, J.; Tai, Y. C.; Laforest, R.; Siegel, B. A.; Welch, M. J., $^{18}$F-fluoroacetate: a potential acetate analog for prostate tumor imaging--in vivo evaluation of $^{18}$F-fluoroacetate versus $^{11}$C-acetate. *J. Nucl. Med.* **2007,** *48*, 420–428.

47. Mori, W.; Takei, M.; Furutsuka, K.; Fujinaga, M.; Kumata, K.; Muto, M.; Ohkubo, T.; Hashimoto, H.; Tamagnan, G.; Higuchi, M.; Kawamura, K.; Zhang, M. R., Comparison between [$^{18}$F]fluorination and [$^{18}$F]fluoroethylation reactions for the synthesis of the PDE10A PET radiotracer [$^{18}$F]MNI-659. *Nucl. Med. Biol.* **2017,** *55*, 12–18.

48. Iwata, R.; Furumoto, S.; Pascali, C.; Bogni, A.; Ishiwata, K., Radiosynthesis of O-[C-11]methyl-L-tyrosine and O-[F-18]fluoromethyl-L-tyrosine as potential PET tracers for imaging amino acid transport. *J. Labelled. Compd. Rad.* **2003,** *46*, 555–566.

49. Wilson, A. A.; Jin, L.; Garcia, A.; DaSilva, J. N.; Houle, S., An admonition when measuring the lipophilicity of radiotracers using counting techniques. *Appl. Radiat. Isot.* **2001,** *54*, 203–208.

50. Pike, V. W., PET radiotracers: crossing the blood-brain barrier and surviving metabolism. *Trends. Pharmacol. Sci.* **2009,** *30*, 431–440.

51. Zhang, M. R.; Tsuchiyama, A.; Haradahira, T.; Yoshida, Y.; Furutsuka, K.; Suzuki, K., Development of an automated system for synthesizing $^{18}$F-labeled compounds using [$^{18}$F]fluoroethyl bromide as a synthetic precursor. *Appl. Radiat. Isot.* **2002,** *57*, 335–342.

52. Zhang, M. R.; Suzuki, K., [$^{18}$F]Fluoroalkyl agents: synthesis, reactivity and application for development of PET ligands in molecular imaging. *Curr. Top. Med. Chem.* **2007,** *7*, 1817–1828.

53. Fujinaga, M.; Yamasaki, T.; Yui, J.; Hatori, A.; Xie, L.; Kawamura, K.; Asagawa, C.; Kumata, K.; Yoshida, Y.; Ogawa, M.; Nengaki, N.; Fukumura, T.; Zhang, M. R., Synthesis and evaluation of novel radioligands for positron emission tomography imaging of metabotropic glutamate receptor subtype 1 (mGluR1) in rodent brain. *J. Med. Chem.* **2012,** *55*, 2342–2352.

54. Fujinaga, M.; Ohkubo, T.; Yamasaki, T.; Zhang, Y.; Mori, W.; Hanyu, M.; Kumata, K.; Hatori, A.; Xie, L.; Nengaki, N.; Zhang, M. R., Automated synthesis of (rac)-, (R)-, and (S)-[$^{18}$F]epifluorohydrin and their application for developing PET radiotracers containing a 3-[$^{18}$F]fluoro-2-hydroxypropyl moiety. *ChemMedChem.* **2018,** 13, 1723–1731.

55. Rami-Mark, C.; Zhang, M. R.; Mitterhauser, M.; Lanzenberger, R.; Hacker, M.; Wadsak, W. [$^{18}$F]FMeNER-D2: reliable fully-automated synthesis for visualization of the norepinephrine transporter. *Nucl. Med. Biol.* **2013,** 40, 1049–1054.

56. Coskran, T. M.; Morton, D.; Menniti, F. S.; Adamowicz, W. O.; Kleiman, R. J.; Ryan, A. M.; Strick, C. A.; Schmidt, C. J.; Stephenson, D. T. Immunohistochemical localization of phosphodiesterase 10A in multiple mammalian species. *J. Histochem. Cytochem.* **2006,** 54, 1205–1213.

57. Seeger, T. F.; Bartlett, B.; Coskran, T. M.; Culp, J. S.; James, L. C.; Krull, D. L.; Lanfear, J.; Ryan, A. M.; Schmidt, C. J.; Strick, C. A.; Varghese, A. H.; Williams, R. D.; Wylie, P. G.; Menniti, F. S. Immunohistochemical localization of PDE10A in the rat brain. *Brain. Res.* **2003,** 985, 113–126.

58. Toth, M.; Haggkvist, J.; Stepanov, V.; Takano, A.; Nakao, R.; Amini, N.; Miura, S.; Kimura, H.; Taniguchi, T.; Gulyas, B.; Halldin, C. Molecular imaging of PDE10A knockout mice with a novel PET radiotracer: [$^{11}$C]T-773. *Mol. Imaging Biol.* **2015,** 17, 445–449.

59. Lammertsma, A. A.; Hume, S. P., Simplified reference tissue model for PET receptor studies. *Neuroimage.* **1996,** *4*, 153–158.

60. Zhang, M. R.; Maeda, J.; Ogawa, M.; Noguchi, J.; Ito, T.; Yoshida, Y.; Okauchi, T.; Obayashi, S.; Suhara, T.; Suzuki, K., Development of a new radioligand, N-(5-fluoro-2-phenoxyphenyl)-N-(2-[$^{18}$F]fluoroethyl-5-methoxybenzyl)acetamide, for PET imaging of peripheral benzodiazepine receptor in primate brain. *J. Med. Chem.* **2004,** *47*, 2228–2235.

61. Takano, A.; Halldin, C.; Varrone, A.; Karlsson, P.; Sjoholm, N.; Stubbs, J. B.; Schou, M.; Airaksinen, A. J.; Tauscher, J.; Gulyas, B., Biodistribution and radiation dosimetry of the norepinephrine transporter radioligand (S,S)-[$^{18}$F]FMeNER-D2: a human whole-body PET study. *Eur. J. Nucl. Med. Mol. Imaging.* **2008,** *35*, 630–636.

62. Stabin, M. G.; Sparks, R. B.; Crowe, E., OLINDA/EXM: the second-generation personal computer software for internal dose assessment in nuclear medicine. *J. Nucl. Med.* **2005,** *46*, 1023–1027.

Table of Content Graphic